# Master Thesis

Solving Cahn-Hilliard equation using a CutCIP method

**Isak Hammer**

Supervisor: André Massing

May 15, 2023

Department of Mathematical Sciences
Norwegian University of Science and Technology

# 1 Introduction

The first application of the Cahn-Hilliard (CH) problem appeared when modelling phase separation of two-component incompressible fluids [1–3], but was quickly generalized to handle multi-component system as well [4–7]. In engineering, CH is the critical component in the phase-field model, a mathematical framework to model transitions and interface dynamics in materials and fluid dynamics [8, 9]. From this, the equation found many interesting applications for a wide variety of problems. To mention a few, we have multiphase fluid dynamical problems [10–13], solidification of binary or multi-component alloys [14, 15], and continuum modelling of fracture dynamics in materials [16, 17]. Perhaps an unexpected application is that CH can be used for in painting when recovering damaged parts of an image [4, 18–20] and modelling the origin of the irregular structure in Saturn's rings [21]. CH is also essential in many areas of biology and medicine. For example, from a macroscopic viewpoint, CH is a great tool to model tumour growth, wound healing and brain tumours [22, 23]. On the microscopic level on the biomembrane, there is an ongoing debate about the existence of the accumulation of lipids into so-called lipid rafts, which serve as a rigid platform for proteins with special properties such as signalling and intercellular trafficking [24–27]. It turns out that the hypothesis can be tested by modelling the problem as a separation problem using CH [28–30].

## 1.1 The Cahn Hilliard Problem

The CH problem comes in many variants depending on its application, but we will in this report on the binary mixture version [7]. Let $\Omega \subset \mathbb{R}^d$ be a compact set for $d = 2, 3$ with a sufficiently smooth boundary $\Gamma$, see Figure 1. We define the time duration parameter $T \in [0, \infty)$ and the so-called unknown phase-field function as the mapping $u : [0, T] \times \Omega \to [-1, 1]$, which is denoted as the local difference of a binary mixture of two concentrations $c_A, c_B \in [0, 1]$ s.t. $u = c_A - c_B$ and $c_A + c_B = 1$. Remark that if a local point exists so $u$ has the extreme value $-1$, then it implies that the particular point has 100% concentration $c_A$ and vice-versa for $c_B$. On the other hand, if $u$ is zero, it implies that the mixture is $50\% - 50\%$.

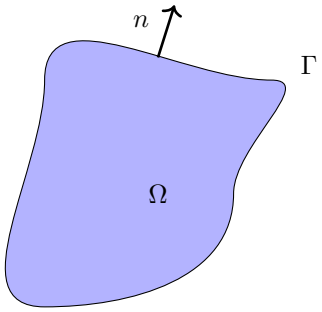


Figure 1: Illustration of the physical domain $\Omega$ for $d = 2$ , the boundary $\Gamma$ and the corresponding normal vector $n$.

For an isotropic binary mixture non-uniform, the standard Ginzburg-Landay free energy functional is given by

$$E(u) = \int_\Omega \frac{\varepsilon^2}{2} |\nabla u|^2 + F(u) dx$$

The nonlinear function $F(u)$ is denoted as the (Helmholtz) free energy density associated with the interaction dynamics between the components and thus comes in many forms depending on the thermodynamic properties, see [7]. However, we will in this article assume that $F(u) = (1/4)(1 - u^2)^4$. We choose to define the chemical potential $\mu$ as the variational derivative,

$$\mu = \frac{\delta E(u)}{\delta u} = f(u) - \varepsilon^2 \Delta c.$$

where we used the notation $f(u) = F'(u)$. First of all, to require local mass conservation, we may enforce the continuity equation, that is

$$\partial_t u + \nabla \cdot \mathcal{J} = 0,$$

where $J$ denotes the flux governed by the physical dynamics. Hence, this naturally leads to the no-flux and the Neumann boundary conditions,

$$\begin{aligned} \mathcal{J} \cdot n &= 0 \text{ on } \Gamma \\ \partial_n u &= 0 \text{ on } \Gamma \end{aligned} \tag{1}$$

A well-accepted law for the flux is that it is proportional to the chemical energy gradient, $\mathcal{J} = -M\nabla\mu$ for a parameter $M$. Thus, we finally have the strong form Cahn-Hilliard equation. Let $u(x,0) = u_0$ then is the dynamics on the form,

$$\begin{aligned} \partial_t u = \Delta(f(u) - \varepsilon^2 \Delta u) \quad &\text{in } \Omega \\ \partial_n u = 0 \quad &\text{on } \Gamma \\ \partial_n (f(u) - \varepsilon^2 \Delta u) = 0 \quad &\text{on } \Gamma \end{aligned} \tag{2}$$

Based on these laws and the boundary conditions, it becomes evident that the energy functional serves as a Lyapunov function in the sense that its time derivative is monotonically decreasing and that the global mass concentration is zero, i.e.

$$\frac{d}{dt} E(u) \leq 0 \text{ and } \frac{d}{dt} \int_\Omega u dx = 0.$$

Remark that the inequality computation utilizes the assumption of $M$ to be constant, and both equations require the no-flux boundary condition, $\mathcal{J} \cdot n = 0$. For details, see [31, Equation 17 ] and [32, Equation 1.7]. This is useful since we expect $E(u(\cdot, t_2)) \leq E(u(\cdot, t_1))$ for $0 < t_1 < t_2$ and that the global mass is conserved,

$$\int_\Omega u(x,t) dx = \int_\Omega u_0(x) dx.$$

The properties under consideration serve as a theoretical foundation for establishing the existence, uniqueness, and long-term behaviour of the CH problem. Consequently, these properties are well-comprehended from a mathematical standpoint. For references, see [33–35].

## 1.2 Numerical Methods

One of the key challenges with the CH problem is that it involves fourth-order spatial derivatives. It has, for simple domains, successfully been implemented using Finite Difference Methods [36, 37] and Spectral Methods [38, 39]. However, these methods are generally constrained to simple domains (with some notable exceptions [40–42]).

As a further evolution to address the CH problem, it is common to consider a corresponding biharmonic (BH) problem as a numerical testbed in the spatial direction. This problem is defined as follows,

$$\begin{aligned} \alpha u + \Delta^2 u = f(x) \quad &\text{in } \Omega, \\ \partial_n u = g_1(x) \quad &\text{on } \Gamma, \\ \partial_n \Delta u = g_2(x) \quad &\text{on } \Gamma. \end{aligned} \tag{3}$$

Here is the functions a mapping $f, g_1, g_2 : \Omega \to \mathbb{R}$ and the constant $\alpha$ is a real number s.t. $\alpha > 0$. The BH problem holds relevance since it is provide a proper spatial-integration test framework prior to moving on solving the non-linearities and time-integration.

The early Finite Element Methods (FEM) for CH were proposed in [35, 43] utilizing global $C^1$ and $C^2$ in one spatial dimension, but later it has been shown that making $C^1$ (or higher order) elements are far from trivial. For reference, see [44–46].

There exist several promising alternative methods that guarantee $C^1$ continuity, and these have shown potential for solving the CH problem. A notable mention is isogeometric analysis (IGA), a technique that leverages Non-Uniform Rational B-Splines (NURBS) to efficiently handle complex geometries and smooth boundaries without the need for mesh refinement. Thus, IGA makes a desirable alternative for problems dealing with intricate and smooth domains [47]. Specifically for the CH problem, has IGA successfully been implemented [48, 49]. Recent results have shown that investigations on unfitted versions of IGA [50] and its applicability to moving surfaces [51] also is possible. Another

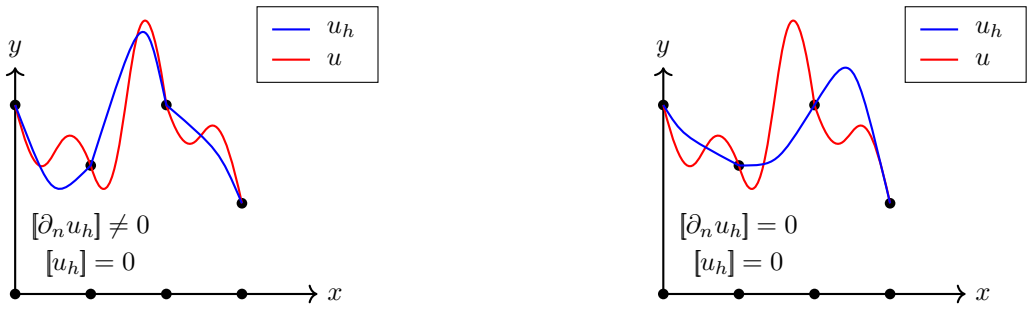


Figure 2: Illustration of global $C^0$ continuous elements (left) and global $C^1$ elements (right) in 1 dimension. Here is $u$ the exact solution and $u_h$ the approximated solution. We define the jump between the elements as $[\![u_h]\!] = u_+ - u_-$.

rising method is the virtual finite element method (VFEM), which has applied so-called virtual $C^1$ elements to handle the continuity requirement [52].

An alternative approach is to avoid global $C^1$ continuity weakend it to global $C^0$ continuity, see Figure 2 . As a result, this strategy has led to the development of two distinct families of methods for solving the CH problem. The first involves the Continuous Interior Penalty (CIP) methods, which uses the standard weak formulation but penalizes the discontinuity of the derivative between elements as a form of regularization. The method has been designed for several interesting stable variants for the BH problem, that is [53–57]. This method is advantageous due to its symmetry and relationship with discontinuous Galerkin (DG) methods [58], renowned for their natural way of handling inhomogeneous boundary conditions, flexibility with unstructured meshes, efficient parallelization, and strong stability. This connection lends robust stability analysis tools, making the method highly suitable for intricate computational problems. The CIP formulation has also then been adapted to solve CH by applying the Newton-Raphson scheme to handle the non-linearities [59] or utilizing an implicit-explicit (IMEX) time integration scheme, where the stiff part is treated implicitly (such as backward Euler) and the nonlinear part explicitly (such as the forward Euler or explicit Runge-Kutta) [60].

Another popular variant is to rewrite the BH problem as a system of second-order problems in a mixed formulation. This strategy not only broadens the problem's flexibility but also provides a more natural means to incorporate boundary conditions, see [61–64]. This approach also leverages the general saddle point theory for mixed FEM methods, which provide a mathematical framework to ensure numerical stability [65]. Moreover, this approach adapts well to the CH problem [59, 66], and some methods even apply a so-called convex splitting scheme approach in a way that preserves the convexity of the energy functional, making the system easier to solve [67, 68]. A combination of these methods, the DG and mixed formulation for the CH problem, has recently been considered [69, 70].

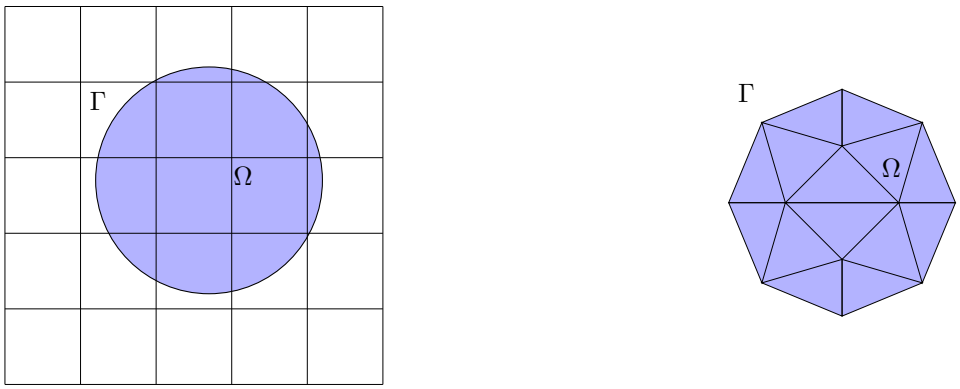


Figure 3: Mesh comparison: unfitted mesh (left) adheres to domain and boundary, while fitted mesh (right) employs a triangular mesh for polygonal approximation of the circular domain.

Creating a high-quality mesh in 2- and 3-dimensional for realistic problems is a challenging task that can take a reasonable time in the simulation workflow and is hard to scale properly on distributed platforms and thus not that suitable for moving domains, very complex meshes or smooth boundaries. An interesting class to approach the problem is the so-called unfitted finite element method, which utilizes a background mesh and does not align with the physical boundary. For an illustration see Figure 3. This greatly reduces the need to generate an unstructured mesh and makes it very applicable for parallelization and moving domains since it avoids the need of remeshing entirely. However, without paying attention to the so-called cut cells, which are the elements intersecting with the boundary, the method quickly leads to instability and ill-conditioning. One of the methods to counter this is the cut finite element method (CutFEM), where the focus is to penalize the cut-cells weakly by adding an additional ghost penalty term to ensure stability and well-posedness [71]. This has been successfully implemented for the BH problem for the mixed formulation [72] and the CIP formulation [73]. However, both implementations are considering an interface problem between two domains. Specifically for the CH problem, the mixed formulation [74] has been shown to be successful. Aggregated unfitted finite element method (AgFEM) is a close relative to CutFEM and has also shown to be promising [75, 76]. The method is an alternative way to the ghost penalty, which instead applies a so-called cell aggregation with respect to a cut cell ( assuming each cell has enough support with interior elements) and, thus, the badly cut cells are removed, ensuring robustness and well-posedness.

### 1.3 Outline of the report

This report is a novel stabilized cut continuous interior penalty method (CutCIP) that utilizes the CutFEM framework to handle complex domains and the CIP formulation for its elegant formulation to handle fourth-order spatial derivatives, to solve the CH problem. We will name the cut continuous interior penalty method (CutCIP) method. In the first section prove that the method is stable and has optimal convergence for the BH problem, and then extend the method to handle the CH problem. We will then provide numerical examples.

## 2 Cut Continuous Interior Penalty Method for the Biharmonic Problem

### 2.1 Notation

We will in this report assume $\Omega$ to be a compact and open set in $\mathbb{R}^d$. Let $p \in \mathbb{R}$, $1 \leq p \leq \infty$. We define the space $L^p(\Omega)$ to be the set of all measurable functions $f : \Omega \mapsto \mathbb{R}$ such that $|f|^p$ is Lebesgue measurable, i.e,

$$L^p(\Omega) = \left\{ f : \Omega \mapsto \mathbb{R} \mid \int_\Omega |f|^p \, d\Omega < \infty \right\}.$$

Let $u \in L^p(\Omega)$. We define the integral norm of order $p$ to be

$$\|u\|_{L^p(\Omega)} = \left( \int_\Omega |u|^p \, dx \right)^{\frac{1}{p}}.$$

Since $p = 2$ is frequently used in this report, we also define for convenience a compact notation $\|u\|_\Omega = \|u\|_{L^2(\Omega)}$ . We say that $L^2(\Omega)$ is a Hilbert space if it is equipped with a inner product of two functions $u, v \in L^2(\Omega)$ s.t. $(u, v)_\Omega = (u, v)_{L^2(\Omega)} = \int_\Omega uv dx$. We now use this notation for derivatives,

$$\partial^\alpha f = \frac{\partial^{|\alpha|} f}{\partial^{\alpha_1} x_1 \partial^{\alpha_2} x_2}, \quad \text{for } \alpha = (\alpha_1, \alpha_2) \text{ and } f \in C^{|\alpha|}(\Omega). \tag{4}$$

For $d$ dimensions of order $k$ we define the multi-index $\alpha = (\alpha_1, \ldots, \alpha_d)$ with the absolute value $|\alpha| = \sum_i \alpha_i = k$ s.t.

$$\partial^\alpha f = \frac{\partial^{\alpha_1}}{\partial x_1^{\alpha_1}} \cdots \frac{\partial^{\alpha_d}}{\partial x_d^{\alpha_d}} f$$

Let $m \geq 0$ be an integer and let $1 \leq p \leq \infty$ be a real number. Then we define the Sobolev space

$$H^m(\Omega) = \left\{ u \in L^2(\Omega) \mid \partial^\alpha u \in L^2(\Omega) \, \forall \alpha : |\alpha| \leq m \right\}.$$

Equipped with the inner product is $H^m(\Omega)$ denoted as a Hilbert space, that is, for $u, v \in H^m(\Omega)$,

$$(u,v)_{H^m(\Omega)} = \sum_{|\alpha| \leq m} \int_\Omega \partial^\alpha u \partial^\alpha v dx.$$

Similarly, the norm is is denoted as, $\|u\|^2_{H^m(\Omega)} = \|u\|^2_{L^2(\Omega)} + \sum_{k=1}^m |u|^2_{H^k(\Omega)}$, where the seminorm is defined such that, $|u|^2_{H^k(\Omega)} = \sum_{|\alpha|=k} \|\partial^\alpha u\|^2_\Omega$. We will often denote the shorthand notation $\|u\|_{k,\Omega} = \|u\|_{H^k(\Omega)}$ and $|u|_{k,\Omega} = |u|_{H^k(\Omega)}$.

## 2.2 Computational Domains

Assume that $\Omega \subset \mathbb{R}^d$ is a compact set with a boundary $\Gamma$. In standard FEM methods a key assumption is that the set $\Omega$ is a polyhedra. This is useful since a polyhedra can be fully covered by a collection of polyhedra and, hence, motivating us to define a fitted mesh. We define a fitted mesh $\mathcal{T}$ of the domain $\Omega$ to be a collection of disjoint polyhedra $\{T\}$ forming a partition of $\Omega$ s.t $\overline{\Omega} = \bigcup_{T \in \mathcal{T}} T$, for illustration see Figure 3. Here we say that each $T \in \mathcal{T}$ is a mesh element or an element. The mesh size is defined as the maximum diameter $h := h_{max}$ of any polyhedra in the mesh $\mathcal{T} = \{T\}$, that is, $h_{max} = \max_{T \in \mathcal{T}} h_T$ s.t. $h_T = diam(T) = \max_{x_1, x_2 \in T} dist(x_1, x_2)$ Hence, motivating us to use the notation $\mathcal{T}_h$ for a mesh $\mathcal{T}$ with size $h$. A mesh is conform if $T_1 \neq T_2$ then $T_1 \cap T_2 \neq \emptyset$ for all $T_1, T_2 \in \mathcal{T}_h$. This means that each $T$ share either a vertex or a facet. Let the chunkiness parameter $c_T := h_T / r_T$, where $r_T$ is the largest ball that be inscribed inside a element $T \in \mathcal{T}_h$. A mesh is said to be shape regular if $c_T \leq c$ is independent of $T$ and $h$. We also say that the mesh is quasi-uniform only if it is shape regular and $h_{max} \leq c h_{min}$. In this report will we assume that a mesh $\mathcal{T}_h$ is conform, shape regular and quasi-uniform unless specified. The fact that the mesh is conform makes is a useful property since the interface between mesh elements has come into contact in the sense that it is either a vertex or a facet. This with the combination of shape regularity and quasi-uniformity has been a major key to prove important inequalities in broken Sobolev spaces [77, Chapter 1.4.1]. Hence, the assumptions are very handy when proving convergence.

Remove introduction of unfitted mesh until later

Questions arise when we want to allow for complex geometries where some physical domain $\Omega$ has a smooth boundary $\Gamma$ and, thus, cannot be fully covered of a fitted mesh. This motivates us to define a so-called unfitted mesh. Let a background domain $\widetilde{\Omega} \subset \mathbb{R}^d$ have a corresponding mesh $\widetilde{\mathcal{T}_h}$. Assume that the physical domain is the set $\Omega \subset \widetilde{\Omega}$ with the corresponding smooth boundary $\Gamma$. We define the unfitted mesh or the active mesh as the triangulation that intersects the interior of $\Omega$, i.e., the intersection $\widetilde{\mathcal{T}_h} \cap Int(\Omega)$ where $Int(\Omega) = \Omega \setminus \Gamma$.

Let $\mathcal{T}_h = \{T\}$ be a mesh of $\Omega \subset \mathbb{R}^d$ consisting of polygons $T \in \mathbb{R}^d$. The set of all facets is the union of external and internal facets, $\mathcal{F}_h = \mathcal{F}_h^{ext} \cup \mathcal{F}_h^{int}$, where each are defined like this:

$$\mathcal{F}_h^{int} = \left\{ F = T^+ \cap T^- \mid T^+, T^- \in \mathcal{T}_h \right\} \text{ and } \mathcal{F}_h^{ext} = \left\{ F = \partial T \cap \partial \Omega \mid T \in \mathcal{T}_h \right\}.$$

Let $\mathcal{T}_h$ be a mesh of $\Omega$ equipped with the facets $\mathcal{F}_h$. We will define the following normal vectors

1) We define $n|_T$ to be unit outward normal on $\partial T$ for each $T \in \mathcal{T}_h$

2) For all $F \in \mathcal{F}_h^{int}$ we define $n$ to be the facet normal $n|_F = n|_{T^+}$ from $T^+$ to $T^-$, illustrated in figure 4.

3) For all $F \in F_h^{ext}$ we define the facet normal $n|_F = n|_T$ to the unit outward normal.

Keep in mind that in many that we often will simply use the notation $n = n|_T$ in most cases.

Let $v \in L^2(\Omega)$ be a scalar function on $\Omega$ with a corresponding shape regular and quasi-uniform mesh $\mathcal{T}_h$. We will use the following definitions.

1) Let $F \in \mathcal{F}_h^{int}$ and $v^\pm|_F = \lim_{t \to 0} v(x \pm tn)$ for $x \in F$. We define the mean as $\{\!\{v\}\!\}|_F = \frac{1}{2}(v_F^+ + v_F^-)$ and the jump as $[\![v]\!]|_F = v_F^+ - v_F^-$.

2) Let $F \in \mathcal{F}_h^{ext}$ and let $v(x) = v(x)|_F$ for $x \in F$. We define the mean as $\{\!\{v\}\!\}|_F = v$ and the jump as $[\![v]\!]|_F = v$.

To simplify will we use the notation $\{\!\{v\}\!\} = \{\!\{v\}\!\}|_F$ and $[\![v]\!] = [\![v]\!]|_F$ for all $F \in \mathcal{F}_h$. Remark that if we have to functions $u, v \in L^2(\mathcal{T}_h)$, then the following identity holds $[\![uv]\!] = [\![u]\!]\{\!\{v\}\!\} + \{\!\{u\}\!\}[\![v]\!]$.

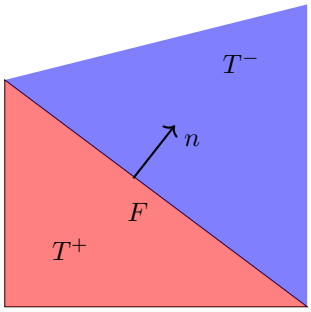


Figure 4: Facet $F \in \mathcal{F}_h^{int}$ shared by the triangles $T^+, T^- \in \mathcal{T}_h$ and the normal unit vector $n$.

## 2.3 Continuous Interior Penalty Method

**Assumption 2.1.** *Assume that any mesh $\mathcal{T}_h$ is conform, shape regular and quasi-uniform.*

Let $\Omega = \mathcal{T}_h \subseteq \mathbb{R}^d$ be a polygonal mesh and $\Gamma$ be a sufficiently smooth boundary.

## 2.4 Initial discrete formulation

We want to make a CutFEM version of the CIP problem. Let $\widetilde{\mathcal{T}_h}$ be a shape-regular and quasi-uniform background mesh. Let us denote the active set $\mathcal{T}_h \subseteq \widetilde{\mathcal{T}_h}$ which intersects the interior of the active domain $\Omega$, that is

$$\mathcal{T}_h = \left\{ T \in \widetilde{\mathcal{T}_h} \mid T \cap (\Omega \setminus \Gamma) \neq \emptyset \right\}.$$

With a corresponding set of interior facets,

$$\mathcal{F}_h = \left\{ F = T^+ \cap T^- \mid T^+, T^- \in \mathcal{T}_h \right\},$$

and a set of cut elements

$$\mathcal{T}_\Gamma = \left\{ T \in \mathcal{T}_h \mid T \cap \Gamma \neq \emptyset \right\}.$$

For convenience, will we define also the interior of the active set as $\mathcal{T}_{int}$.

$$\mathcal{T}_{int} = \left\{ T \in \mathcal{T}_h \mid T \cap Int(\Omega) \neq \emptyset \right\}.$$

Hence, we have that the active set is the union of the interior and cut elements, $\mathcal{T}_h = \mathcal{T}_{int} \cap \mathcal{T}_\Gamma$. For an illustration, see figure.

We denote the $C^0$ polynomial space of order $k$ as

$$V_h = \left\{ v \in C^0(\Omega) : v_T = v|_T \in \mathcal{P}^k(T), \forall T \in \mathcal{T}_h \right\}$$

From the previous chapter can we write the CIP method. The bilinear form $a_h : V_h \times V_h \to \mathbb{R}$ is defined as

$$\begin{aligned} a_h(u,v) = &(\alpha u, v)_{\mathcal{T}_h \cap \Omega} + \left(D^2 u, D^2 v\right)_{\mathcal{T}_h \cap \Omega} \\ &+ \left(\{\!\{\partial_{nn} u\}\!\}, [\partial_n v]\right)_{\mathcal{F}_h \cap \Omega} + \left(\{\!\{\partial_{nn} v\}\!\}, [\partial_n u]\right)_{\mathcal{F}_h \cap \Omega} \\ &+ (\partial_{nn} u, \partial_n v)_\Gamma + (\partial_{nn} v, \partial_n u)_\Gamma \\ &+ \frac{\gamma}{h}\left([\partial_n u], [\partial_n v]\right)_{\mathcal{F}_h \cap \Omega} + \frac{\gamma}{h}\left(\partial_n u, \partial_n v\right)_\Gamma \end{aligned}. \tag{5}$$

Similarly the linear form is defined as

$$l_h(v) = (f, v)_{\mathcal{T}_h \cap \Omega} - (g_2, v) - (g_1, \partial_{nn} v)_\Gamma + \frac{\gamma}{h}(g_1, \partial_n v).$$

To make sure the problem is stabilized will we add a ghost-penalty. That is, we define the discrete problem to find a $u_h \in V_h$ s.t.

$$A_h(u_h, v) := a_h(u_h, v) + g_h(u_h, v) = l_h(v) \quad \forall v \in V_h.$$

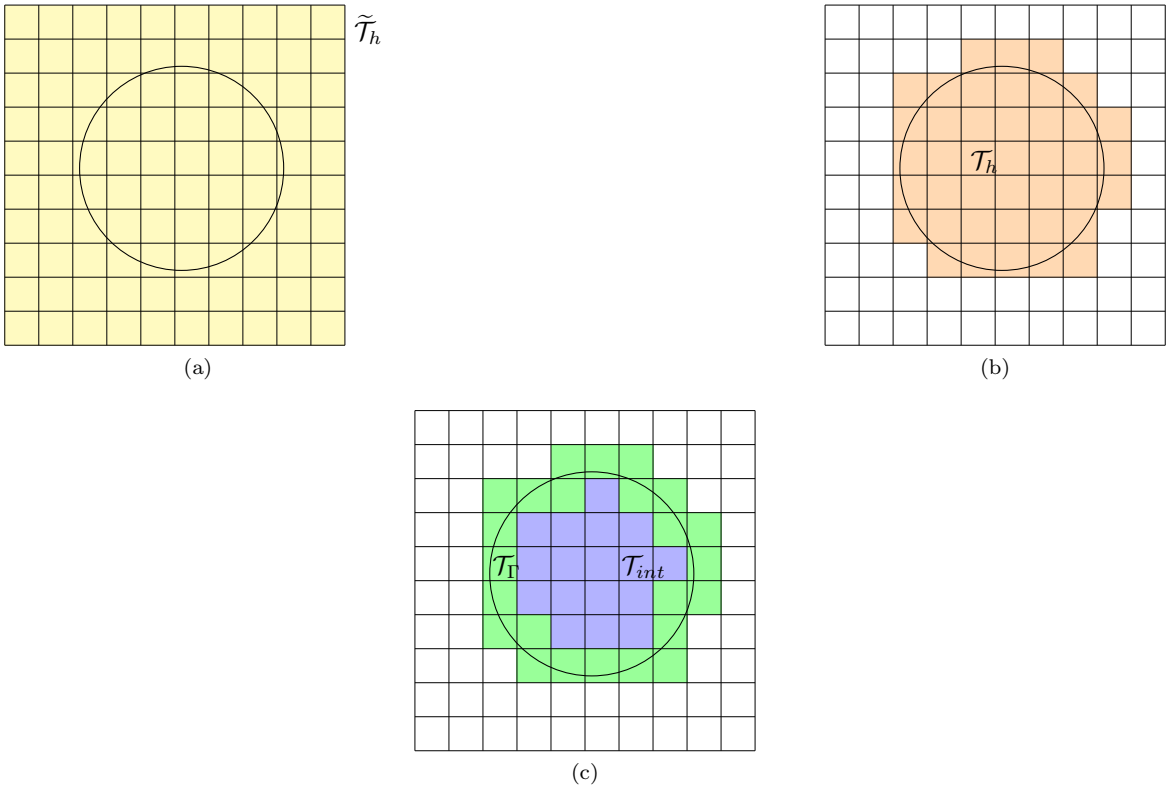


(a) (b) (c)

Figure 5: Illustration of the background mesh $\widetilde{T}_h$, the active set $\mathcal{T}_h$, the cut cells $\mathcal{T}_\Gamma$ and the interior of the active set $\mathcal{T}_{int}$

We define the underlying norms for $v \in V_h$ as

$$\|v\|_{a_h}^2 = \||\alpha|^{\frac{1}{2}} v\|_{\mathcal{T}_h \cap \Omega}^2 + \|D^2 v\|_{\mathcal{T}_h \cap \Omega}^2 + \gamma \|h^{-\frac{1}{2}} [\![\partial_n v]\!]\|_{\mathcal{F}_h \cap \Omega}^2 + \gamma \|h^{-\frac{1}{2}} \partial_n v\|_\Gamma^2, \tag{6}$$

$$|v|_{g_h}^2 = g(v, v) \tag{7}$$

$$\|v\|_{A_h}^2 = \|v\|_{a_h}^2 + |v|_{g_h}^2 \tag{8}$$

$$\tag{9}$$

and for $v \in V + V_h$ we get,

$$\|v\|_{a_h,*}^2 = \|v\|_{a_h}^2 + \|h^{\frac{1}{2}} \{\!\{\partial_{nn} v\}\!\}\|_{\mathcal{F}_h \cap \Omega}^2 + \|h^{\frac{1}{2}} \partial_{nn} v\|_\Gamma^2$$

$$\|v\|_{A_h,*}^2 = \|v\|_{a_h,*}^2 + |v|_{g_h}^2$$

*Remark.* Note that it holds that $\mathcal{T}_h \cap \Omega = \Omega$ and $\mathcal{T}_h \cap \Gamma = \Gamma$. Depending on context, we choose the best suitable notation.

## 2.5 Stability estimate

Similarly for the Poisson problem will we have the following assumptions for the computational mesh;

**S.1** Boundary $\Gamma$ is of $C^2$

**S.2** The mesh $\mathcal{T}_h$ is quasi-uniform.

**S.3** For a $T \in \mathcal{T}_\Gamma$ there exists a path $P$ of $diam(P) \lesssim h$ which contains $T$ and an element $T'$ with a so-called fat intersection $|T' \cap \Omega|_d \geq |T'|_d$.

From basic theory we have the following inverse estimate for $v \in \mathcal{P}^k(T)$ s.t.

$$\|\partial_{nn} v\|_F \lesssim \|h_T^{-\frac{1}{2}} D^2 v\|_T,$$

where the hidden constant depend on dimension $d$, order $k$ and the shape regularity. Similarly for cut elements is it easy to see that this must hold,

$$\|\partial_{nn} v\|_{F\cap\Omega} \lesssim \|\partial_{nn} v\|_F \lesssim \|h_T^{-\frac{1}{2}} D^2 v\|_T.$$

A useful variant is the following inequality that is,

$$\|\partial_{nn} v\|_{\Gamma\cap T} \lesssim h^{-\frac{1}{2}} \|D^2 v\|_T.$$

Summation the inverse inequalities over $\mathcal{F}_h$ and $\mathcal{T}_h$ implies that

$$\|\partial_{nn} v\|_{\mathcal{T}_h\cap\Gamma} \lesssim h^{-\frac{1}{2}} \|D^2 v\|_{\mathcal{T}_h}, \tag{10}$$

$$\|\partial_{nn} v\|_{\mathcal{F}_h\cap\Omega} \lesssim h^{-\frac{1}{2}} \|D^2 v\|_{\mathcal{T}_h}. \tag{11}$$

In fact, combining the inequalities we get the identity,

$$h\|\partial_{nn} v\|^2_{\mathcal{F}_h\cap\Omega} + h\|\partial_{nn} v\|^2_{\mathcal{T}_h\cap\Gamma} \lesssim \|D^2 v\|^2_{\mathcal{T}_h}. \tag{12}$$

We may introduce our first assumption on the ghost penalty.

**Assumption 2.2** (EP1)**.** *The ghost penalty $g_h$ extends the $H^1$ norm s.t.*

$$\|D^2 v\|^2_{\mathcal{T}_h} \lesssim \|D^2 v\|^2_\Omega + |v|^2_{g_h}.$$

Combing the results we get the following convenient corollary.

**Corollary 2.1.** *Let $g_h$ satisfy Assumption 2.2 then*

$$h\|\partial_{nn} v\|^2_{\mathcal{F}_h\cap\Omega} + h\|\partial_{nn} v\|^2_{\mathcal{T}_h\cap\Gamma} \lesssim \|D^2 v\|^2_\Omega + |v|^2_{g_h} \lesssim \|v\|^2_{A_h}$$

*Proof.* The first inequality is a direct result of (12) and Assumption 2.2. The second inequality is simply a results of the definition (8). □

**Lemma 2.1.** *The discrete form $A_h$ is coercive, that is,*

$$\|v\|^2_{A_h} \lesssim A_h(v,v) \forall v \in V_h$$

*Proof.* Let $v \in V^h$. Observe that

$$A_h(v,v) = a_h(v,v) + |v|^2_{g_h}$$

Thus, since the second term already is part of the $\|\cdot\|_{A_h}$ norm is a good start to focus on the $a_h$ term, that is,

$$\begin{aligned} a_h(v,v) = \| \, |\alpha|^{\frac{1}{2}} \cdot v\|^2_\Omega + \|D^2 v\|^2_\Omega + 2(\{\!\{\partial_{nn} v\}\!\}, [\partial_n v])_{\mathcal{F}_h\cap\Omega} + 2(\partial_{nn} v, \partial_n v)_\Gamma \\ + \frac{\gamma}{h}\| \, [\partial_n v] \, \|^2_{\mathcal{F}_h} + \frac{\gamma}{h}\|\partial_n v\|^2_\Gamma \end{aligned}$$

We will first focus on the symmetry terms. Using Cauchy-Schwarz we observe that

$$\begin{aligned} (\{\!\{\partial_{nn} v\}\!\}, [\partial_n v])_{\mathcal{F}_h\cap\Omega} &\geq -\|h^{\frac{1}{2}} \{\!\{\partial_{nn} v\}\!\} \|_{\mathcal{F}_h\cap\Omega} \|h^{-\frac{1}{2}} [\partial_n v] \|_{\mathcal{F}_h\cap\Omega} \\ (\partial_{nn} v, \partial_n v)_\Gamma &\geq -\|h^{\frac{1}{2}} \partial_{nn} v\|_\Gamma \|h^{-\frac{1}{2}} \partial_n v\|_\Gamma \end{aligned}$$

Using inverse-inequalities (10) and (11) and the Corollary 2.1 can we easily observe that

$$\begin{aligned} \| \{\!\{\partial_{nn} v\}\!\} \|^2_{\mathcal{T}_h\cap\Omega} \leq C_1 \|D^2 v\|^2_{\mathcal{T}_h} \leq C(\|D^2 v\|^2_\Omega + |v|^2_{g_h}) \\ \|\partial_{nn} v\|^2_\Gamma \leq C_2 \|D^2 v\|^2_{\mathcal{T}_h} \leq C(\|D^2 v\|^2_\Omega + |v|^2_{g_h}) \end{aligned}$$

Thus, by applying Youngs $\varepsilon$-inequality, $2ab \leq \varepsilon^{-1} a^2 + \varepsilon b^2$, is it natural to see that,

$$\begin{aligned} -C_1^{\frac{1}{2}} \|D^2 v\|_{\mathcal{T}_h} \|h^{-\frac{1}{2}} [\partial_n v] \|_{\mathcal{F}_h\cap\Omega} \geq -\frac{1}{\varepsilon} C(\|D^2 v\|^2_\Omega + |v|^2_{g_h}) - \varepsilon \|h^{-\frac{1}{2}} [\partial_n v] \|^2_{\mathcal{F}_h\cap\Omega} \\ -C_2^{\frac{1}{2}} \|D^2 v\|_{\mathcal{T}_h} \|h^{-\frac{1}{2}} \partial_n v\|_\Gamma \geq -\frac{1}{\varepsilon} C(\|D^2 v\|^2_\Omega + |v|^2_{g_h}) - \varepsilon \|h^{-\frac{1}{2}} \partial_n v\|^2_\Gamma \end{aligned}$$

Combining these ideas do we end up with the following inequality,

$$\begin{aligned} a_h(v,v) \geq \| \, |\alpha|^{\frac{1}{2}} \, v\|_\Omega^2 + \|D^2 v\|_\Omega^2 - \frac{1}{\varepsilon} 4C(\|D^2 v\|_\Omega^2 + |v|_{g_h}^2) \\ + (\gamma - 2\varepsilon)\left(\|h^{-\frac{1}{2}} \left[\partial_n v\right] \|_{\mathcal{F}_h \cap \Omega}^2 + \|h^{-\frac{1}{2}} \partial_n v\|_\Gamma^2\right) \end{aligned}$$

This inequality is useful, since if we apply it on the $\|\cdot\|_{A_h}$ we have a extra ghost penalty term s.t.,

$$\begin{aligned} A_h(v,v) &= a(v,v) + |v|_{g_h}^2 \\ &\geq \| \, |\alpha|^{\frac{1}{2}} \, v\|_\Omega^2 + (1 - \frac{1}{\varepsilon} 4C)(\|D^2 v\|_\Omega^2 + |v|_{g_h}^2) \\ &+ (\gamma - 2\varepsilon)\left(\|h^{-\frac{1}{2}} \left[\partial_n v\right] \|_{\mathcal{F}_h \cap \Omega}^2 + \|h^{-\frac{1}{2}} \partial_n v\|_\Gamma^2\right). \end{aligned}$$

Setting $\varepsilon = 8C$ and $C = \frac{\gamma}{32}$ we simplify the problem to

$$\begin{aligned} A_h(v,v) &\geq \| \, |\alpha|^{\frac{1}{2}} \, v\|_\Omega^2 + \frac{1}{2}(\|D^2 v\|_\Omega^2 + |v|_{g_h}^2) \\ &\quad + \frac{\gamma}{2}\left(\|h^{-\frac{1}{2}} \left[\partial_n v\right] \|_{\mathcal{F}_h \cap \Omega}^2 + \|h^{-\frac{1}{2}} \partial_n v\|_\Gamma^2\right) \\ &\gtrsim \|v\|_{A_h}^2 \end{aligned}$$

Hence, proof is complete. □

**Lemma 2.2.** *The discrete form $A_h$ is bounded, that is,*

$$A_h(v,w) \lesssim \|v\|_{A_h} \|v\|_{A_h} \forall w \in V_h \tag{13}$$

*Moreover, for $v \in V_h + V$ and $w \in V_h$ the discrete form $a_h$ satisfies*

$$a_h(v,w) \lesssim \|v\|_{a_h,*} \|w\|_{A_h} \tag{14}$$

*Proof.* We will divide the proof in two steps.

1) The goal is to prove the inequality (13).

$$|A_h(v,w)| \lesssim |a_h(v,w)| + |g_h(v,w)|$$

By assumption is the ghost penalty $g_h$ positive semi-definite, thus, it fulfills the Cauchy-Schwartz inequality

$$|g_h(v,w)| \lesssim |v|_{g_h} |w|_{g_h}$$

Hence, by definition is $|g_h(v,w)| \lesssim \|v\|_{A_h} \|w\|_{A_h}$. Now it remains to show that the bilinear term $a_h$ is bounded.

$$\begin{aligned} |a_h(v,w)| \leq &\left|(\alpha v, w)_{\mathcal{T}_h \cap \Omega}\right| + \left|\left(D^2 v, D^2 w\right)_{\mathcal{T}_h \cap \Omega}\right| \\ &+ \left|\left(\{\!\{\partial_{nn} v\}\!\}, [\partial_n w]\right)_{\mathcal{F}_h \cap \Omega}\right| + \left|\left(\{\!\{\partial_{nn} v\}\!\}, [\partial_n w]\right)_{\mathcal{F}_h \cap \Omega}\right| \\ &+ |(\partial_{nn} v, \partial_n w)_\Gamma| + |(\partial_{nn} w, \partial_n v)_\Gamma| \\ &+ \frac{\gamma}{h}\left|\left([\partial_n v], [\partial_n w]\right)_{\mathcal{F}_h \cap \Omega}\right| + \frac{\gamma}{h}\left|(\partial_n v, \partial_n w)_\Gamma\right| \end{aligned} \tag{15}$$

The strategy is to bound each term individually using Cauchy-Schwartz. We can easily see that $\left|(\alpha v, w)_{\mathcal{T}_h \cap \Omega}\right| \lesssim \|v\|_{a_h} \|w\|_{a_h}$ and that $\left|\left(D^2 v, D^2 w\right)_{\mathcal{T}_h \cap \Omega}\right| \lesssim \|v\|_{a_h} \|w\|_{a_h}$ using Cauchy Schwartz. For the symmetric terms we also apply the inverse inequality (11).

$$\begin{aligned} \left|\left(\{\!\{\partial_{nn} v\}\!\}, [\partial_n w]\right)_{\mathcal{F}_h \cap \Omega}\right| &\lesssim \| \, \{\!\{\partial_{nn} v\}\!\} \, \|_{\mathcal{F}_h \cap \Omega} \| \, [\partial_n w] \, \|_{\mathcal{F}_h \cap \Omega} \\ &\lesssim \|h^{\frac{1}{2}} \partial_{nn} v\|_{\mathcal{F}_h \cap \Omega} \|h^{-\frac{1}{2}} \left[\partial_n w\right] \|_{\mathcal{F}_h \cap \Omega} \\ &\lesssim \|v\|_{A_h} \|w\|_{a_h} \end{aligned}$$

Here we used the Corollary 2.1 s.t. $\|h^{\frac{1}{2}}\partial_{nn}v\|_{\mathcal{F}_h\cap\Omega} \lesssim \|v\|_{A_h}$. The boundedness interior penalty inequality is showed in this manner,

$$\frac{\gamma}{h}\left|\left([\![\partial_n v]\!],[\![\partial_n w]\!]\right)_{\mathcal{F}_h\cap\Omega}\right| \lesssim \|h^{-\frac{1}{2}}[\![\partial_n v]\!]\|_{\mathcal{F}_h\cap\Omega}\|h^{-\frac{1}{2}}[\![\partial_n w]\!]\|_{\mathcal{F}_h\cap\Omega} \lesssim \|v\|_{a_h}\|w\|_{a_h}.$$

Now it remains to handle boundary terms.

$$|(\partial_{nn}v,\partial_n w)_\Gamma| \lesssim \|h^{\frac{1}{2}}\partial_{nn}v\|_\Gamma\|h^{-\frac{1}{2}}\partial_n w\|_\Gamma \lesssim \|v\|_{A_h}\|w\|_{a_h}$$

Again, here we used the Corollary 2.1. Finally, using the definition of the norm is it easily to see that,

$$\frac{\gamma}{h}|(\partial_n v,\partial_n w)_\Gamma| \lesssim \gamma\|h^{-\frac{1}{2}}\partial_n v\|_\Gamma\|h^{-\frac{1}{2}}\partial_n w\|_\Gamma \lesssim \|v\|_{a_h}\|w\|_{a_h}.$$

Obviously is $\|v\|_{a_h} \lesssim \|v\|_{A_h}$. Hence, we have showed that all terms in $a_h$ is bounded in the $\|\cdot\|_{A_h}$ norm.

2) The goal is to prove (14) using many of the same ideas as in the first part. Let $v \in V_h + V$ and $v \in V_h$. Next step is to show that the bilinear term $a_h$ is bounded.

$$\begin{aligned}|a_h(v,w)| \leq\ & \left|(\alpha v,w)_{\mathcal{T}_h\cap\Omega}\right| + \left|\left(D^2v,D^2w\right)_{\mathcal{T}_h\cap\Omega}\right| \\ &+ \left|\left(\{\!\{\partial_{nn}v\}\!\},[\![\partial_n w]\!]\right)_{\mathcal{F}_h\cap\Omega}\right| + \left|\left(\{\!\{\partial_{nn}w\}\!\},[\![\partial_n v]\!]\right)_{\mathcal{F}_h\cap\Omega}\right| \\ &+ |(\partial_{nn}v,\partial_n w)_\Gamma| + |(\partial_{nn}w,\partial_n v)_\Gamma| \\ &+ \frac{\gamma}{h}\left|\left([\![\partial_n v]\!],[\![\partial_n w]\!]\right)_{\mathcal{F}_h\cap\Omega}\right| + \frac{\gamma}{h}|(\partial_n v,\partial_n w)_\Gamma|\end{aligned} \tag{16}$$

We can easily observe from the first part that this must holds,

$$\left|(\alpha v,w)_{\mathcal{T}_h\cap\Omega}\right| + \left|\left(D^2v,D^2w\right)_{\mathcal{T}_h\cap\Omega}\right| \lesssim \|v\|_{a_h,*}\|w\|_{A_h}.$$

And for the symmetric interior terms,

$$\begin{aligned}\left|\left(\{\!\{\partial_{nn}v\}\!\},[\![\partial_n w]\!]\right)_{\mathcal{F}_h\cap\Omega}\right| &\lesssim \|h^{\frac{1}{2}}\{\!\{\partial_{nn}v\}\!\}\|_{\mathcal{F}_h\cap\Omega}\|h^{-\frac{1}{2}}[\![\partial_n w]\!]\|_{\mathcal{F}_h\cap\Omega} \lesssim \|v\|_{a_h,*}\|w\|_{A_h}, \\ \left|\left(\{\!\{\partial_{nn}w\}\!\},[\![\partial_n v]\!]\right)_{\mathcal{F}_h\cap\Omega}\right| &\lesssim \|h^{\frac{1}{2}}\{\!\{\partial_{nn}w\}\!\}\|_{\mathcal{F}_h\cap\Omega}\|h^{-\frac{1}{2}}[\![\partial_n v]\!]\|_{\mathcal{F}_h\cap\Omega} \lesssim \|w\|_{A_h}\|v\|_{a_h,*}.\end{aligned}$$

Remark that for $\|h^{\frac{1}{2}}\{\!\{\partial_{nn}v\}\!\}\|_{\mathcal{F}_h\cap\Omega}$ is the norm incorporated in the definition of $\|\cdot\|_{a_h,*}$, but for $\|h^{\frac{1}{2}}\{\!\{\partial_{nn}w\}\!\}\|_{\mathcal{F}_h\cap\Omega}$ was the Corollary 2.1 applied. The jump terms $\|h^{-\frac{1}{2}}[\![\partial_n v]\!]\|_{\mathcal{F}_h\cap\Omega}$ is incorporated in the $\|\cdot\|_{a_h}$ norm, thus, this also holds,

$$\frac{\gamma}{h}\left|\left([\![\partial_n v]\!],[\![\partial_n w]\!]\right)_{\mathcal{F}_h\cap\Omega}\right| \lesssim \|h^{-\frac{1}{2}}[\![\partial_n v]\!],\|_{\mathcal{F}_h\cap\Omega}\|h^{-\frac{1}{2}}[\![\partial_n w]\!]\|_{\mathcal{F}_h\cap\Omega} \lesssim \|v\|_{a_h,*}\|w\|_{A_h}$$

Finally, the boundary terms,

$$\begin{aligned}(\partial_{nn}v,\partial_n w)_\Gamma &\lesssim \|h^{\frac{1}{2}}\partial_{nn}v\|_\Gamma\|h^{-\frac{1}{2}}\partial_n w\|_\Gamma \lesssim \|v\|_{a_h,*}\|w\|_{A_h}, \\ (\partial_{nn}w,\partial_n v)_\Gamma &\lesssim \|h^{\frac{1}{2}}\partial_{nn}w\|_\Gamma\|h^{-\frac{1}{2}}\partial_n v\|_\Gamma \lesssim \|w\|_{A_h}\|v\|_{a_h,*},\end{aligned}$$

and

$$\frac{\gamma}{h}\left|(\partial_n v,\partial_n w)_{\mathcal{F}_h\cap\Omega}\right| \lesssim \|h^{-\frac{1}{2}}\partial_n v\|_\Gamma\|h^{-\frac{1}{2}}\partial_n w\|_\Gamma \lesssim \|v\|_{a_h,*}\|w\|_{A_h},$$

where we just applied the definition of the norms $\|\cdot\|_{a_h}$ and $\|\cdot\|_{a_h,*}$. We have now shown that every term is bounded.

Hence, the proof is complete. □

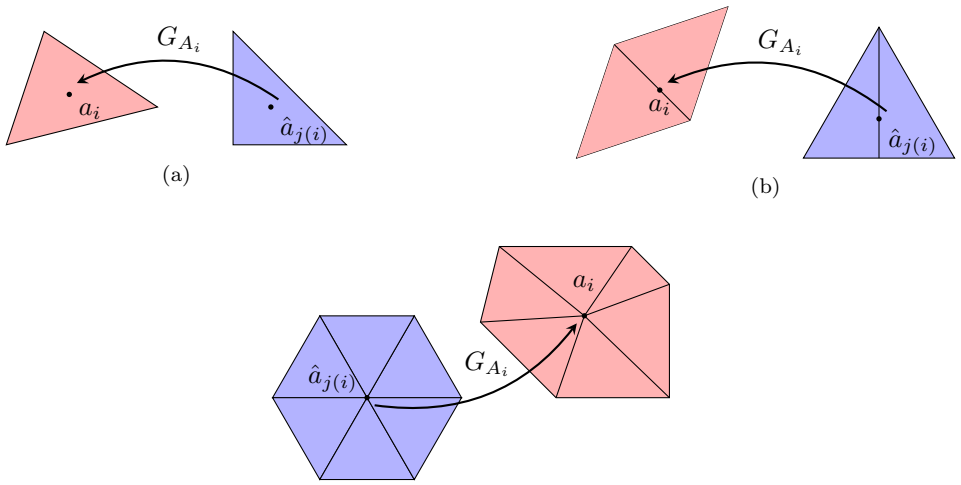


Figure 6: Illustration of the different cases when mapping from the reference macroelement $\widehat{A}_{j(i)}$ to the domain $A_i$, $G_{A_i} : \widehat{A}_{j(i)} \to A_i$. Here we have defined $\hat{a}_{j(i)} \in \widehat{A}_{j(i)}$ s.t. $G(\hat{a}_{j(i)}) = a_i$.

## 2.6 A priori estimates

In this section will we do only a brief overview of the important assumptions and definitions required to prove optimal convergence. Recall that for $v \in H^1(\mathcal{T}_h)$ these inequalities holds $\forall T \in \mathcal{T}_h$ s.t.

$$\|v\|_{\partial T} \lesssim h_T^{-\frac{1}{2}} \|v\|_T + h^{\frac{1}{2}} \|\nabla v\|_T,$$
$$\|v\|_{\Gamma \cap T} \lesssim h^{-\frac{1}{2}} \|v\|_T + h_T^{\frac{1}{2}} \|\nabla v\|_T.$$

For proof, see [78, Lemma 4.2].

### 2.6.1 Cléments interpolation

We want to compute the expected convergence rate of the energy norm (8). An important tool in the process is the Cléments interpolation operator, $C_h$. It is used for interpolation on non smooth functions by applying an regularization on so-called macroelements. Let us denote the $\mathcal{P}_c^k(\Omega)$ to be an $H^1$ conformal polynomial space. We denote $\{a_1, \ldots, a_N\}$ to be the Lagrange nodes. Associated with each node $a_i$ we denote the macroelement $A_i$ to consist of all simplices containing $a_i$. Let $n_{cf}$ be the number of configurations for the macroelement, then we define the index $j : \{1, \ldots, N\} \to \{1, \ldots, n_{cf}\}$ s.t. $j(i)$ is the index associated with the reference configuration $\widehat{A}_{j(i)}$ for corresponding macroelement $A_i$ for an illustration, see Figure 6.

Let us define a $C^0$-diffeomorphism $G_{A_i} : \widehat{A}_{j(i)} \to A_i$ s.t. for all $\widehat{T} \in \widehat{A}_{j(i)}$ is the restriction $G_{A_i|\widehat{T}}$ affine. The Cléments interpolation operator $C_h$ is defined as a $L^2$-projection onto the macroelements. That is, given a reference macroelement $\widehat{A}_{j(i)}$ and a function $\hat{v} \in L^1(\widehat{A}_{j(i)})$, then $\widehat{C}_{j(i)}\hat{v}$ is the unique polynomial in $\mathcal{P}^k(\widehat{A}_{j(i)})$ s.t.

$$\int_{\widehat{A}_{j(i)}} (\widehat{C}_{j(i)}\hat{v} - \hat{v}) p \, dx = 0 \quad \forall p \in \mathcal{P}^k(\widehat{A}_{j(i)})$$

Finally, we define the Cléments interpolator $C_h : L^1(\Omega) \to \mathcal{P}_c^k(\Omega)$ s.t.

$$C_h v = \sum_{i=1}^{N} \widehat{C}_{j(i)}(v(G_{A_i})(G_{A_i}^{-1}(a_i)))\phi_i,$$

where $\phi_i$ is the corresponding polynomial basis at node $a_i$.

Recall the integral norm notation,

$$\|u\|_{m,p,T} = \left( \sum_{|\alpha| \leq m} \int_T |\partial^\alpha u|^p \, dx \right)^{\frac{1}{2}}$$

where we use that $\|u\|_T = \|u\|_{m,0,T}$ and similarly $\|u\|_{2,T} = \|u\|_{m,2,T}$.

We denote a patch, $\omega(T)$, as the set of elements in $\mathcal{T}_h$ sharing at least one vertex with $T \in \mathcal{T}_h$ . And similarly we denote a another patch, $\omega(F)$, as the set of all elements in $\mathcal{T}_h$ sharing at least one vertex with $F \in \mathcal{F}_h$.

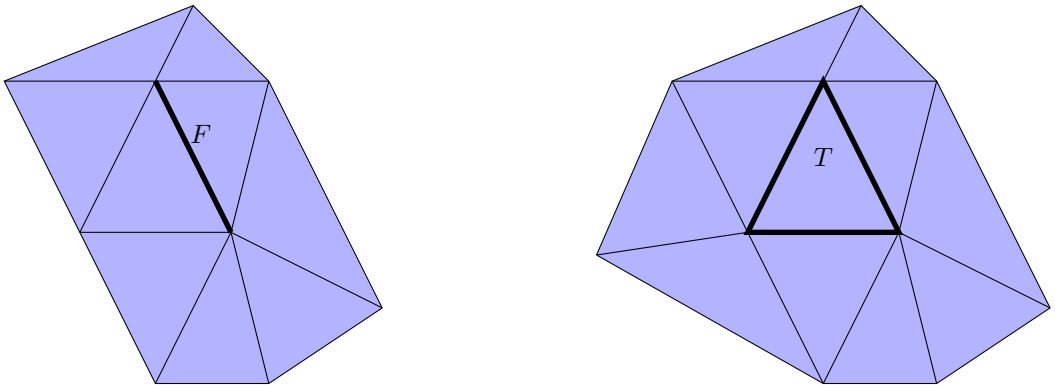


Figure 7: Illustration of patch $\omega(F)$ on left side and $\omega(T)$ on the rights side.

Finally, we have the following lemma

**Lemma 2.3.** *We define the Clement interpolation as the projection $C_h : H^m(\Omega) \mapsto V_h$, where $V_h$ has the order $k$. Then does the following stability estimate hold,*

$$\|C_h v\|_{H^m(\Omega)} \lesssim \|v\|_{H^m(\Omega)} \quad \forall v \in H^m(\Omega),$$

*and if the following conditions for an parameter $l$ is satisfied, it exists error estimates s.t.,*

$$m \leq l \leq k+1 \implies \|v - C_h v\|_{m,p,T} \lesssim h_T^{l-m} \|v\|_{l,p,\omega(T)} \quad \forall T \in \mathcal{T}_h, \forall v \in H^l(\omega(T)),$$
$$m + \frac{1}{2} \leq l \leq k+1 \implies \|v - C_h v\|_{m,p,F} \lesssim h_T^{l-m-\frac{1}{2}} \|v\|_{l,p,\omega(F)} \quad \forall \partial T \in \mathcal{T}_h, \forall v \in H^l(\omega(F)).$$

Why first $C_h : L^1 \to \mathcal{P}^k$ and now $C_h : H^m \to \mathcal{P}^k$?

**Corollary 2.2.** *Let $0 \leq l \leq k+1$ and let $0 \leq m \leq \min(1, l)$. Given Lemma 2.3 then there exists an $C > 0$ s.t.*

$$\inf_{v_h \in \mathcal{P}_c^k(\Omega)} \|v - v_h\|_{m,p,\Omega} \leq C h^{l-m} \|v\|_{l,p,\Omega} \forall v \in W_{l,p}(\Omega).$$

This result is very useful since it is now sufficient to show that a priori estimates holds given to prove convergence rate.

For further detailed information, please investigate [79, Chapter 1.6]. We will use these estimates to compute convergence rate given that Ceas' Lemma holds.

### 2.6.2 Energy a priori estimates.

A key idea is to distinguish between the physical space $\Omega$ and the polyhedra consisting of the active mesh $\Omega_h^e = \mathcal{T}_h$. Thus, to do an a priori estimate we find it necessary to define an bounded extension operator satisfying,

$$(\cdot)^e : W^{m,q}(\Omega) \to W^{m,q}(\Omega^e), \quad \|v^e\|_{m,q,\Omega^e} \lesssim \|v\|_{m,q,\Omega}.$$

where $0 < m \leq \infty$ and $1 \leq q \leq \infty$.

The physical space $\Omega$ is a subset of $\Omega^e$, so I do not understand why $\|v^e\|_{m,q,\Omega^e} \lesssim \|v\|_{m,q,\Omega}$ should hold.

Now assume that $\Omega_h^e \subset \Omega^e$. We define an unfitted Cléments interpolator $C_h^e : H^r(\Omega_h^e) \to V_h$ s.t. $C_h^e v := C_h v^e$. We can immediately observe that the interpolation satisfies the global error estimates,

that is,

$$\|v - C_h^e v\|_{r,\mathcal{T}_h} \lesssim h^{s-r} \sum_{T\in\mathcal{T}_h} \|v\|_{s,\omega(T)}, \quad 0 \le r \le s \tag{17}$$

$$\|v - C_h^e v\|_{r,\mathcal{F}_h} \lesssim h^{s-r-\frac{1}{2}} \sum_{T\in\mathcal{T}_h} \|v\|_{s,\omega(F)}, \quad 0 \le r \le s - \frac{1}{2} \tag{18}$$

$$\|v - C_h^e v\|_{r,\Gamma} \lesssim h^{s-r-\frac{1}{2}} \sum_{T\in\mathcal{T}_h} \|v\|_{s,\omega(T)}, \quad 0 \le r \le s - \frac{1}{2} \tag{19}$$

Naturally can we see this is the tools we need to construct an estimate for the energy norm.

**Lemma 2.4.** *Let $u \in H^s(\Omega)$ for $s \ge 3$ be a solution of (??). Then we have*

$$\|u - C_h u\|_{a_h,*} \lesssim h^{s(s-2)} \|u\|_{H^s(\Omega)}$$

*Proof.* By definition is

$$\begin{aligned}\|u - C_h^e u\|_{a_h,*}^2 = {} & \||\alpha|^{\frac{1}{2}}(u - C_h^e u)\|_{\mathcal{T}_h\cap\Omega}^2 + \|D^2(u - C_h^e u)\|_{\mathcal{T}_h\cap\Omega}^2 \\ & + \gamma\|h^{-\frac{1}{2}} [\![\partial_n(u - C_h^e u)]\!] \|_{\mathcal{F}_h\cap\Omega}^2 + \gamma\|h^{-\frac{1}{2}}\partial_n(u - C_h^e u)\|_{\Gamma}^2 \\ & + \|h^{\frac{1}{2}} \{\!\{\partial_{nn}(u - C_h^e u)\}\!\} \|_{\mathcal{F}_h\cap\Omega}^2 + \|h^{\frac{1}{2}}\partial_{nn}(u - C_h^e u)\|_{\Gamma}^2.\end{aligned}$$

The strategy is to bound each term individually by applying the estimates (17), (18) and (18).

1) Starting with the first term we get

$$\||\alpha|^{\frac{1}{2}}(u - C_h^e u)\|_{\mathcal{T}_h\cap\Omega}^2 \le \|\alpha\|_{L^\infty(\Omega)}^2 \|(u - C_h^e u)\|_{0,\mathcal{T}_h}^2 \lesssim h^{2s} \sum_{T\in\mathcal{T}_h} \|v\|_{s,w(T)}^2$$

Here we simply used (17).

2) Similarly can we use for the second term,

$$\|D^2(u - C_h^e u)\|_{\mathcal{T}_h\cap\Omega}^2 \lesssim \|u - C_h^e u\|_{2,\mathcal{T}_h}^2 \lesssim \sum_{T\in\mathcal{T}_h} h^{2(s-2)} \|u\|_{s,\omega(T)}^2.$$

Again, this is via the estimate (17).

3) Recall $\|[\![u]\!]\|_{\mathcal{F}_h} \le \|v^+\|_{\mathcal{F}_h} + \|v^-\|_{\mathcal{F}_h} \lesssim \|u\|_{\partial\mathcal{T}_h}^2$ and the inverse estimate $\|\partial_n u\|_F \lesssim h^{-\frac{1}{2}}\|\nabla u\|_T$. Hence, by (18)

$$\begin{aligned}\gamma\|h^{-\frac{1}{2}} [\![\partial_n(u - C_h^e u)]\!] \|_{\mathcal{F}_h\cap\Omega}^2 &\lesssim \|h^{-\frac{1}{2}}\partial_n(u - C_h^e u)\|_{\partial\mathcal{T}_h}^2 \lesssim h^{-2}\|\nabla(u - C_h^e u)\|_{\mathcal{T}_h}^2 \\ &\lesssim h^{-2}\|u - C_h^e u\|_{1,\mathcal{T}_h}^2 \lesssim \sum_{T\in\mathcal{T}_h} h^{2(s-1)}\|u\|_{s,T}^2\end{aligned}$$

Not sure if (18) holds here!

$$\|\partial_n(u - C_h^e u)\|_{1,\partial\mathcal{T}_h}^2 \lesssim \sum_{T\in\mathcal{T}_h} h^{2(l-m-\frac{1}{2})}\|u\|_{s,\omega(F)}^2$$

4) And for the boundary term we simply apply (19),

$$\gamma\|h^{-\frac{1}{2}}\partial_n(u - C_h^e u)\|_{\Gamma}^2 \lesssim h^{-2}\|\nabla(u - C_h^e u)\|_{\Gamma}^2 \lesssim h^{-2}\|u - C_h^e u\|_{1,\Gamma}^2 \lesssim h^{2(s-r-\frac{1}{2})-2} \sum_{T\in\mathcal{T}_h} \|u\|_{s,T}^2$$

Does it makes sense to integrate $\|\nabla u\|_\Gamma$, i.e. no normal vectors? I guess not. Hence, (19) is kinda strange.

5) We also know that $\| \{\!\{u\}\!\} \|_{\mathcal{F}_h} \leq \|u^+\|_{\mathcal{F}_h} + \|u^-\|_{\mathcal{F}_h} \lesssim \|u\|^2_{\partial\mathcal{T}_h}$ and the $\|\partial_{nn}u\|_F \lesssim h^{-\frac{1}{2}}\|D^2u\|_T$. It is clear by using (18) that this must holds

$$\begin{aligned}\|h^{\frac{1}{2}} \{\!\{\partial_{nn}(u - C_h^e u)\}\!\} \|^2_{\mathcal{F}_h\cap\Omega} &\lesssim h\|\partial_{nn}(u - C_h^e u)\|^2_{\partial\mathcal{T}_h} \lesssim \|D^2(u - C_h^e u)\|^2_{\mathcal{T}_h} \\ &= \|u - C_h^e u\|^2_{2,\mathcal{T}_h} \lesssim h^{2s} \sum_{T\in\mathcal{T}_h} \|u\|_{s,\omega(T)}\end{aligned}$$

6) Similarly we can easily see by using (19) that this must hold,

$$\|h^{\frac{1}{2}}\partial_{nn}(u - C_h^e u)\|^2_\Gamma \lesssim \|D^2(u - C_h^e u)\|^2_\Gamma \lesssim \|u - C_h^e u\|^2_{2,\Gamma} \lesssim h^{2(s-r-\frac{1}{2})} \sum_{T\in\mathcal{T}_h} \|u\|^2_{s,\omega(T)}$$

Finally, combining all the estimates we have

$$\begin{aligned}\|u - C_h^e u\|^2_{a_h,*} \lesssim \sum_{T\in\mathcal{T}_h} \Big( & h^{2s}\|u\|_{s,\omega(T)} + h^{2(s-2)}\|u\|^2_{s,\omega(T)} \\ & + h^{2(s-1)}\|u\|^2_{s,T} + h^{2(s-r-\frac{1}{2})-2}\|u\|^2_{s,T} \\ & + h^{2s}\|u\|_{s,\omega(T)} + h^{2(s-r-\frac{1}{2})}\|u\|^2_{s,\omega(T)} \Big) \\ \lesssim h^{2s(s-2)}\|u\|^2_{H^s(\Omega)}\end{aligned}$$

Thus, the proof is complete.

Cleanup proof

□

**Lemma 2.5** (Weak galerkin orthogonality)**.** *Let $u \in H^s(\Omega)$, $s \geq 3$ be solution to (??) and $u_h \in V_h$ is a discrete solution to (5). Then is*

$$a_h(u - u_h, v) = g_h(u_h, v) \quad \forall v \in V_h.$$

**Assumption 2.3** (EP2)**.** *For $v \in H^s(\Omega)$ and $r = \min\{s, k+1\}$, the semi-norm $|\cdot|_{g_h}$ satisfies the following estimate,*

$$|C_h^e v|_{g_h} \lesssim h^{r-1}\|v\|_{r,\Omega}.$$

**Theorem 2.1.** *Let $u \in H^s(\Omega)$ , $s \geq 3$ be the solution to (??) and let $u \in V_h$ of order $k$ be the solution to (5). Then for $r = \min\{s, k+1\}$ the error $e = u - u_h$ satisfies*

$$\|e\|_{a_h,*} \lesssim h^{r-1}\|u\|_{r,\Omega} \tag{20}$$

$$\|e\|_\Omega \lesssim h^r\|u\|_{r,\Omega} \tag{21}$$

*Proof.* We will divide the proof into two steps.

1) We want to prove that $\|e\|_{a_h,*} \lesssim h^{r-1}\|u\|_{r,\Omega}$. Let $e = u - u_h$ consist of $e = e_h + e_\pi$, where the discrete error has the form $e_h = C_h^e u - u_h$ and the interpolation error $e_\pi = u - C_h^e u$. We can then observe that

$$\|u - u_h\|_{a_h} \leq \|e_\pi\|_{a_h,*} + \|e_h\|_{A_h}$$

Using Lemma 2.4, can we see that $\|e_\pi\|_{a_h,*} \lesssim h^{r-1}\|u\|_{r,\Omega}$ is already fulfilled. So it remains to check the discrete part. From Lemma 2.1, 2.2, the weak Galerkin orthogonality and Assumption 2.3 is it natural to see that,

$$\begin{aligned}\|e_h\|^2_{A_h} &\lesssim a_h(C_h^e u - u_h, e_h) + g_h(C_h^e u - u_h, e_h) \\ &= a_h(C_h^e u - u, e_h) + a_h(u - u_h, e_h) + g_h(C_h^e u - u_h, e_h) \\ &= a_h(C_h^e u - u, e_h) + g_h(C_h^e u, e_h) \\ &\lesssim h^{r-1}\|u\|_{r,\Omega}\|e_h\|_{A_h}.\end{aligned}$$

The last line of the calculations above comes from the fact that

$$\begin{aligned} a_h(C_h^e u - u, e_h) + g_h(C_h^e u, e_h) &\lesssim \|C_h^e u - u\|_{a_h,*}\|e_h\|_{a_h,*} + |C_h^e u|_{g_h}\,|e_h|_{g_h} \\ &\lesssim \|C_h^e u - u\|_{a_h,*}\|e_h\|_{a_h,*} + h^{r-1}\|e_h\|_{r,\Omega}\,|e_h|_{g_h} \\ &\lesssim (\|C_h^e u - u\|_{a_h,*} + h^{r-1}\|e_h\|_{r,\Omega})\|e_h\|_{A_h} \\ &\lesssim h^{r-1}\|u\|_{r,\Omega}\|e_h\|_{A_h}. \end{aligned}$$

Here we noticed that $\|e_h\|_{a_h,*}+|e_h|_{g_h} \lesssim \|e_h\|_{A_h}$. We also argued that $\|C_h^e u-u\|_{a_h,*} \lesssim h^{r-1}\|u\|_{r,\Omega}$ from Lemma 2.4.

TODO: Need to show $\|e_h\|_{a_h,*} + |e_h|_{g_h} \leq \|e_h\|_{A_h}$

Hence, the first part of the proof is complete.

2) We want to show that $\|e\|_\Omega \lesssim h^r\|u\|_{r,\Omega}$. The idea is to apply the so-called Aubin-Nitsche duality trick by being aware of the ghost penalty $g_h$. Let us denote the following observation. Because of the Assumption **EP2** is there a function $\phi \in H^2(\Omega) \cap H_0^1(\Omega)$ and a $\psi \in L^2(\Omega)$ s.t.

$$-\Delta\phi = \psi \text{ and } \|\phi\|_{2,\Omega} \lesssim \|\psi\|_\Omega.$$

Because of the regularity $\phi$ can we write $(e,\psi)_\Omega = (e,-\Delta\phi)_\Omega = a_h(e,\phi)$. Naturally, we can now seek to bound this operator. That is,

$$\begin{aligned} (e,\psi)_\Omega &= a_h(e,\phi) \\ &= a_h(e,\phi - C_h^e\phi) + g_h(u_h - C_h^e u, C_h^e\phi) + g_h(C_h^e u, C_h^e\phi) \\ &\lesssim h^r\|u\|_{r,\Omega}\|\psi\|_\Omega \end{aligned}$$

In the first line we used the weak orthogonality, i.e.,

$$\begin{aligned} a_h(e,\phi) &= a_h(e,\phi - C_h^e\phi) + a_h(u - u_h, C_h^e\phi) \\ &= a_h(e,\phi - C_h^e\phi) + g_h(u_h, C_h^e\phi) \\ &= a_h(e,\phi - C_h^e\phi) + g_h(u_h - C_h^e u, C_h^e\phi) + g_h(C_h^e u, C_h^e\phi). \end{aligned}$$

The last inequality appears after applying Cauchy-Schwartz and Assumption **EP2**.

$$\begin{aligned} &a_h(e,\phi - C_h\phi) + g_h(u_h - C_h^e u, C_h^e\phi) + g_h(C_h^e u, C_h\phi) \\ &\qquad\lesssim \|e\|_{a_h,*}\|\phi - C_h^e\phi\|_{a_h,*} + |\pi_h^e u - u_h|_{g_h}\,|C_h^e\phi|_{g_h} + |C_h^e u|_{g_h}\,|C_h^e\phi|_{g_h} \\ &\qquad. \end{aligned}$$

Using the result from the first part and the Assumption **EP2**.

$$\begin{aligned} \|e\|_{a_h,*} &\lesssim h^{r-1}\|u\|_{r,\Omega} \\ |C_h^e u|_{g_h} &\lesssim h^{r-1}\|u\|_{2,\Omega} \\ |C_h^e u - u_h|_{g_h} &\lesssim \|C_h^e u - u_h\|_{A_h} \\ |C_h^e\phi|_{g_h} &\lesssim \dots \\ \|\phi - C_h^e\phi\|_{a_h,*} &\lesssim \dots \end{aligned}$$

TODO: Finish proof.

□

## 2.7 Constructing Ghost Penalties

We have the following assumptions for the ghost penalty.

**EP1** The ghost penalty $g_h$ extends the $H^1$ norm s.t.

$$\|D^2 v\|^2_{\mathcal{T}_h} \lesssim \|D^2 v\|^2_{\Omega} + |v|^2_{g_h}$$

**EP2** For $v \in H^s(\Omega)$ and $r = \min\{s, k+1\}$, the semi-norm $|\cdot|_{g_h}$ satisfies the following estimate,

$$|\pi_h^e v|_{g_h} \lesssim h^{r-1} \|v\|_{r,\Omega}.$$

We will construct face-based ghost penalties.

**Lemma 2.6.** *Let $T_1, T_2 \in \mathcal{T}_h$ be two elements sharing a common face $F$. Then for $v \in V_h$ we have*

$$\|v\|_{T_1} \lesssim \|v\|_{T_2} \sum_{0 \le j \le k} h^{2j+1} (\left[\!\left[\partial_n^j v\right]\!\right], \left[\!\left[\partial_n^j v\right]\!\right])_F$$

*Proof.* See [80, Lemma 2.19]. □

The goal in this chapter is to engineer an ghost penalty which fulfills these assumptions. We denote the multi-index $\alpha = (\alpha_1, \ldots, \alpha_d)$ of order $|\alpha| = \sum_i \alpha_i = k$ and the normal vectors $n^\alpha = n_1^{\alpha_1} \ldots n_d^{\alpha_d}$. Recall the notation for the derivates $D^\alpha v$ , that is

$$D^0 v = v, \quad D^1 v = \nabla v \text{ and } D^2 v = J(\nabla v) = Hess(v).$$

But $\alpha = (\alpha_1, \ldots, \alpha_d)$ cannot be a scalar? Ex. How can $D^\alpha = D^1$ be a consistent notation.

where $J$ is the Jacobian operator. Remark that equivalent element-wise is the following,

$$[\nabla v]_i = \partial_{x_i} v, \quad \left[D^2 v\right]_{i,j} = \partial_{x_i x_j} v,$$

Let us introduce the notation

$$\partial_n^j v = \sum_{|\alpha|=j}^{k} \frac{D^\alpha v(x) n^\alpha}{\alpha!}, \quad |\alpha| = \sum_{j}^{d} \alpha_i$$

An useful result that may help us design ghost penalty is the following estimate.

**Lemma 2.7.** *Let $T_1, T_2 \in \mathcal{T}_h$ share a common facet $F \in \mathcal{F}_h$. Then for $v \in V_h$ does this hold*

$$\|v\|^2_{T_1} \lesssim \|v\|^2_{T_2} + \sum_{j=0}^{k} h^{2j+1} (\left[\!\left[\partial_n^j v\right]\!\right], \left[\!\left[\partial_n^j v\right]\!\right])_F$$

*Here is $k$ the polynomial degree.*

*Proof.* For a detailed proof, see [80]. □

We will now introduce the so-called ghost penalty faces, that is,

$$\mathcal{F}_h^g = \left\{ F \in \mathcal{F}_h : T^+ \cap \Gamma \neq \emptyset \vee T^- \cap \Gamma \neq \emptyset \right\}.$$

This set is simply all facets that belong to all elements of the active mesh $\mathcal{T}_h$ intersected with $\Gamma$, i.e., all triangles to the cut cells $\mathcal{T}_\Gamma$. For an illustration, see Figure 8.

**Proposition 2.1.** *The following identity holds for $j = 0, 1, 2$.*

$$\partial_n^j (D^2 v) = D^2 (\partial_n^j v)$$

*Proof.* Recall that $\left[D^2 v\right]_{i,j} = \partial_{x_i x_j} v$. We will compute each index individually.

1) $j = 0$ is trivially true.

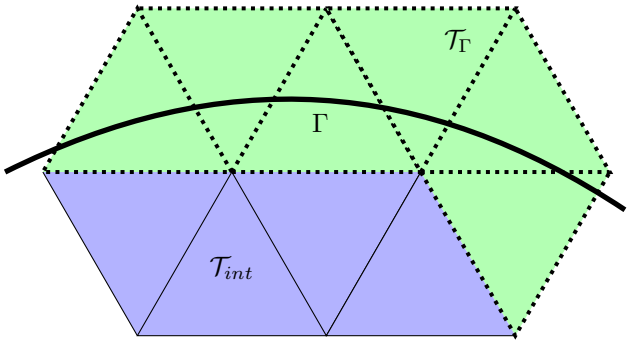


Figure 8: Illustration of $\mathcal{F}_h^g$ denoted as the dotted lines. The set is defined as all facets which belongs to cut cells $\mathcal{T}_\Gamma$ .

2) Let $j = 1$. We can then easily see that,

$$\partial_n(\partial_{x_i x_j} v) = \nabla(\partial_{x_i x_j} v)n = \partial_{x_i x_j}(\nabla v)n = \partial_{x_i x_j}(\partial_n v)$$

Hence, $\partial_n(D^2 v) = D^2(\partial_n v)$.

3) Let $j = 2$. Similarly can we see that,

$$\begin{aligned}\partial_n^2(\partial_{x_i x_j} v) &= n^T D^2(\partial_{x_i x_j} v)n = n^T J(\nabla(\partial_{x_i x_j} v))n \\ &= n^T J(\partial_{x_i x_j}(\nabla v))n = \partial_{x_i x_j} n^T J(\nabla v)n\end{aligned}$$

Thus, taking account for all elements in the matrix we get $\partial_n^2(D^2 v) = D^2(\partial_n^2 v)$.

Proof is complete.

□

**Lemma 2.8.** *Assume **S.2** and **S.3**. For $v \in V_h$ it holds that*

$$\|v\|_{\mathcal{T}_h}^2 \lesssim \|v\|_\Omega^2 + \sum_{j=0}^{k} h^{2j+1}(\left[\!\left[\partial_n^j v\right]\!\right], \left[\!\left[\partial_n^j v\right]\!\right])_{\mathcal{F}_h^g} \tag{22}$$

$$\|D^2 v\|_{\mathcal{T}_h}^2 \lesssim \|D^2 v\|_\Omega^2 + \sum_{j=0}^{k} h^{2j-3}(\left[\!\left[\partial_n^j v\right]\!\right], \left[\!\left[\partial_n^j v\right]\!\right])_{\mathcal{F}_h^g} \tag{23}$$

*Here is $k$ the polynomial degree.*

*Proof.* We will dive the proof in two parts where we first prove (22) and then in the second part prove (23).

1) First of all, notice that there is a patch $P(T)$ consisting of $\{T_i\}_{i=1}^l$ mesh elements s.t. each pair $\{T_i, T_{i+1}\}$ share a facet $F_i$ and the last element $T_l$ has a so-called "fat" intersection according to Assumption **S.3**.

Let us define the following norm

$$g_{F_i}^{L^2}(v, v) = \sum_{j=0}^{k} h^{2j+1}(\left[\!\left[\partial_n^j v\right]\!\right], \left[\!\left[\partial_n^j v\right]\!\right])_{F_i}$$

where $F_i \in \mathcal{F}_h^g$ and polynomial degree $k$. Using Lemma 2.7 can we see that

$$\|v\|_{T_i} \lesssim \|v\|_{T_{i+1}}^2 + g_{F_i}^{L^2}(v, v).$$

Consequently, using induction over each pair $\{T_i, T_{i+1}\}$ with a corresponding $F_i$, we obtain

$$\begin{aligned}\|v\|_{T_1}^2 &\leq C\|v\|_{T_2}^2 + g_{F_1}^{L^2}(v,v)\\ &\leq C(C(\|v\|_{T_3}^2 + g_{F_2}^{L^2}(v,v)) + g_{F_1}^{L^2}(v,v))\\ &\lesssim \|v\|_{T_l}^2 + \sum_{i=1}^{l-1} g_{F_i}^{L^2}(v,v)\\ &\lesssim \|v\|_{T_l\cap\Omega}^2 + \sum_{i=1}^{l-1} g_{F_i}^{L^2}(v,v)\end{aligned}$$

Here the last steps arise from the fact that $\|v\|_{T_l} \lesssim \|v\|_{T_l\cap\Omega}$, which is a consequence of the Assumption **S.3**. Summation over the intersected triangles $\mathcal{T}_\Gamma$ implies,

$$\|v\|_{\mathcal{T}_\Gamma}^2 \lesssim \|v\|_{\mathcal{T}_\Gamma\cap\Omega}^2 + \sum_{i=1}^{l-1} g_{F_l}^{L^2}(v,v) = \|v\|_{\mathcal{T}_\Gamma\cap\Omega}^2 + \sum_{j=0}^{k} h^{2j+1}(\left[\!\left[\partial_n^j v\right]\!\right], \left[\!\left[\partial_n^j v\right]\!\right])_{\mathcal{F}_h^g}$$

And as a trivial extension this now also holds for the active mesh $\mathcal{T}_h$ , that is,

$$\|v\|_{\mathcal{T}_h}^2 \lesssim \|v\|_{\mathcal{T}_h\cap\Omega}^2 + \sum_{j=0}^{k} h^{2j+1}(\left[\!\left[\partial_n^j v\right]\!\right], \left[\!\left[\partial_n^j v\right]\!\right])_{\mathcal{F}_h^g}.$$

Hence, (22) holds and the first part of the proof is complete.

2) We will simply start by replacing $v$ by $D^2 v$ and use the Proposition 2.1.

$$\begin{aligned}\|D^2 v\|_{\mathcal{T}_h}^2 &\lesssim \|D^2 v\|_\Omega^2 + \sum_{j=0}^{k} h^{2j+1}(\left[\!\left[\partial_n^j D^2 v\right]\!\right], \left[\!\left[\partial_n^j D^2 v\right]\!\right])_{\mathcal{F}_h^g}\\ &= \|D^2 v\|_\Omega^2 + \sum_{j=0}^{k} h^{2j+1}(\left[\!\left[D^2\partial_n^j v\right]\!\right], \left[\!\left[D^2\partial_n^j v\right]\!\right])_{\mathcal{F}_h^g}\end{aligned}$$

Remark that $\|D^2 v\|_{T_l} \lesssim \|D^2 v\|_{T_l\cap\Omega}$ also holds based on Assumption **S.3**. Thus, it remains to show that

$$\sum_{j=0}^{k} h^{2j+1}(\left[\!\left[D^2\partial_n^j v\right]\!\right], \left[\!\left[D^2\partial_n^j v\right]\!\right])_{\mathcal{F}_h^g} \lesssim \sum_{j=0}^{k} h^{2j-3}(\left[\!\left[\partial_n^j v\right]\!\right], \left[\!\left[\partial_n^j v\right]\!\right])_{\mathcal{F}_h^g}.$$

Let us denote the tangential operator $P_F := I - n \oplus n$, where $n \oplus n$ is an outer product of the normals on a facet $F$. We apply this so we can to decompose the Hessian evaluated on the facet s.t.

$$D^2 v \mid_F = (\partial_{nn} v)n + P_F D^2 v.$$

Need to find a better version for $(\partial_{nn} v)n$

Recall from basic finite element theory that $\|D^2 v\|_F^2 \leq h^{-2}\|\nabla v\|_F^2 \leq h^{-4}\|v\|_F^2$. That is, applying the decomposition we get the following estimates

$$\|\left[\!\left[P_F D^2 \partial_n^j v\right]\!\right]\|_F^2 = \|P_F D^2 \left[\!\left[\partial_n^j v\right]\!\right]\|_F^2 \lesssim h^{-4}\|\left[\!\left[\partial_n^j v\right]\!\right]\|_F^2.$$

Thus, using this on the decomposition can we admit that

$$\begin{aligned}h^{2j+1}\|\left[\!\left[D^2\partial_n^j v\right]\!\right]\|_F^2 &\lesssim h^{2j+1}\|\partial_{nn}\left[\!\left[\partial_n^j v\right]\!\right] n\|_F^2 + h^{2j+1}\|P_F D^2 \left[\!\left[\partial_n^j v\right]\!\right]\|_F^2\\ &\lesssim h^{2j+1}\|\left[\!\left[\partial_n^{j+2} v\right]\!\right]\|_F^2 + h^{2j-3}\|\left[\!\left[\partial_n^j v\right]\!\right]\|_F^2\end{aligned}$$

Check last argument!

Thus, fulfilling (23).

$$\sum_{j=0}^{k} h^{2j+1}(\left[\!\left[D^2\partial_n^j v\right]\!\right], \left[\!\left[D^2\partial_n^j v\right]\!\right])_{\mathcal{F}_h^g} = \sum_{j=0}^{k} h^{2j+1}\|\left[\!\left[D^2\partial_n^j v\right]\!\right]\|_{\mathcal{F}_h^g}^2$$

TODO: Finish this proof.

□

Finally, we now have the tools we need to construct an candidate for the ghost penalty for which satisfies all assumptions.

**Proposition 2.2** (Face-based ghost penalty)**.** *For any set of positive parameters* $\{\gamma_j\}_{j=0}^k$*, the ghost penalty defined as*

$$g_h(v,w) := \sum_{j=0}^{k} \sum_{F \in \mathcal{F}_h^g} \gamma_j h_F^{2j-3} (\left[\!\left[\partial_n^j v\right]\!\right], \left[\!\left[\partial_n^j w\right]\!\right])_F \text{ for any } v, w \in V_h,$$

*satisfies the Assumption* ***EP1*** *and* ***EP2****.*

*Proof.* First of all, from it is clear that

$$\|D^2 v\|_{\mathcal{T}_h} \lesssim \|D^2 v\|_\Omega + |v|_{g_h}$$

Thus, the Assumption **EP1** is satisfied.

For **EP2** we. □

## 2.8 Results

Since we have in the analysis assumed that $\Gamma$ is $C^2$ will we run our test problems on a circle with radius $r = 1$ with order $k = 2$.

### 2.8.1 Test Problem 1

We introduce the following manufactured solution $u_{ex}(x,y) = (x^2 + y^2 - 1)^2 \sin(2\pi x)\cos(2\pi y)$. To compute the corresponding functions $f, g_1$ and $g_2$ did we use algorithmic differentiation. The method was implemented in Julia using the FEM package Gridap [81, 82]. You can see the corresponding results in Figure 10 and Table 2.

Table 1: Convergence analysis of the numerical method

| $n$ | $\|e\|_{L^2}$ | **EOC** | $\|e\|_{H^1}$ | **EOC** | $\|e\|_{a_h,*}$ | **EOC** | **Cond number** | **ndofs** |
|---|---|---|---|---|---|---|---|---|
| 4 | 4.0E-01 | | 3.6E+00 | | 3.6E+01 | | 1.1E+06 | 8.1E+01 |
| 8 | 1.7E-01 | 1.27 | 1.3E+00 | 1.43 | 2.0E+01 | 0.89 | 3.0E+06 | 2.4E+02 |
| 16 | 2.4E-02 | 2.77 | 2.9E-01 | 2.19 | 9.2E+00 | 1.09 | 1.2E+08 | 8.3E+02 |
| 32 | 6.0E-03 | 2.01 | 7.2E-02 | 2.04 | 4.5E+00 | 1.02 | 3.2E+08 | 3.0E+03 |
| 64 | 2.1E-03 | 1.54 | 1.8E-02 | 1.98 | 2.3E+00 | 1.00 | 4.2E+10 | 1.1E+04 |
| 128 | 5.2E-04 | 2.00 | 4.5E-03 | 2.01 | 1.1E+00 | 1.00 | 4.4E+11 | 4.3E+04 |
| 256 | 8.8E-05 | 2.57 | 1.1E-03 | 2.02 | 5.7E-01 | 1.00 | 2.5E+18 | 1.7E+05 |

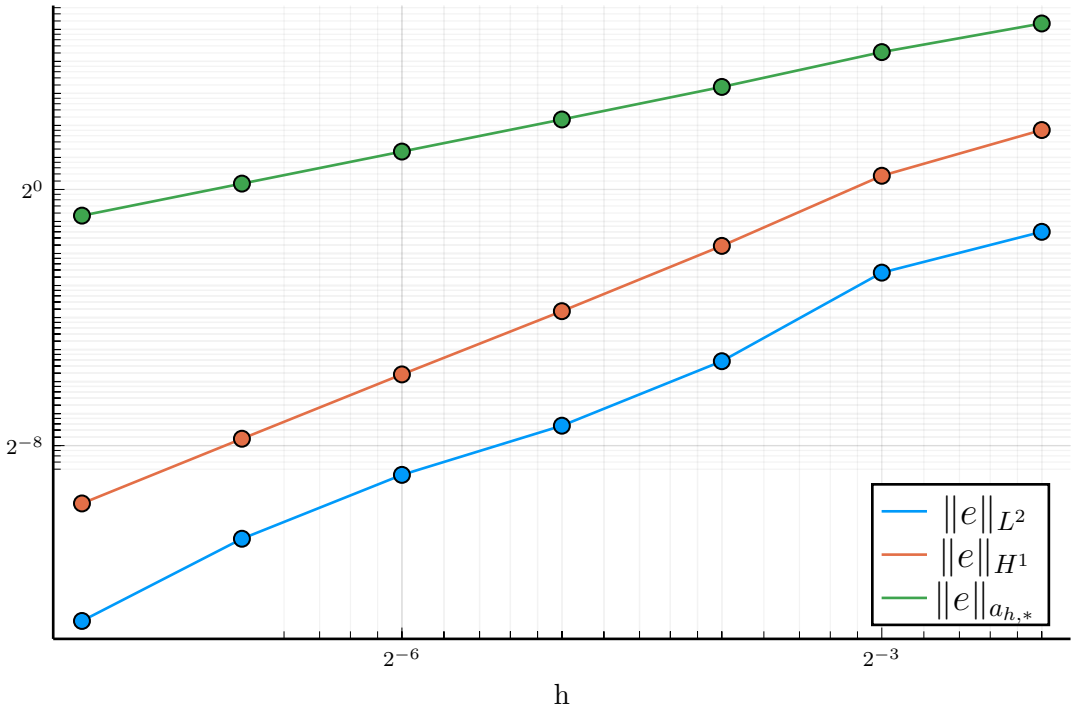


Figure 9: The plot presents the $L^2$ and $H^1$ error norms and the error in the energy norm ($\|e\|_{a_h,*}$).

# 3 Numerical results

Table 2: Convergence analysis of the numerical method

| $n$ | $\|e\|_{L^2}$ | **EOC** | $\|e\|_{H^1}$ | **EOC** | $\|e\|_{a_h,*}$ | **EOC** | **Cond number** | **ndofs** |
|---|---|---|---|---|---|---|---|---|
| 8 | 1.6E+01 | | 1.3E+02 | | 3.6E+03 | | 3.0E+05 | 2.4E+02 |
| 16 | 3.7E+00 | 2.14 | 3.1E+01 | 2.09 | 1.0E+03 | 1.78 | 2.2E+06 | 8.3E+02 |
| 32 | 8.3E-01 | 2.15 | 7.4E+00 | 2.09 | 2.9E+02 | 1.83 | 1.6E+07 | 3.0E+03 |
| 64 | 2.3E-01 | 1.87 | 1.8E+00 | 2.03 | 8.0E+01 | 1.86 | 1.3E+08 | 1.1E+04 |
| 128 | 5.0E-02 | 2.19 | 4.4E-01 | 2.04 | 2.6E+01 | 1.63 | 1.0E+09 | 4.3E+04 |
| 256 | 1.3E-02 | 1.92 | 1.1E-01 | 2.01 | 8.4E+00 | 1.63 | 7.9E+09 | 1.7E+05 |

In this section, we present the numerical results of the convergence analysis for a numerical method applied to a square grid with a length of 1. The grid is discretized with $n = 2^6$ grid points. The analysis is based on a manufactured solution, which is given by the expression:

$$u_{\text{ex}}(x) = 100 \sin\left(\frac{m(2\pi)}{L} x_1\right) \cos\left(\frac{r(2\pi)}{L} x_2\right)$$

Here, $L$, $m$, and $r$ are constants representing the length of the square grid, the spatial frequency in the $x_1$ direction, and the spatial frequency in the $x_2$ direction, respectively.

The convergence analysis involves evaluating the errors in different norms as well as studying the condition number of the system. Table 2 presents the results of the convergence analysis for the numerical method. The column labeled "$n$" corresponds to the number of grid points, while the columns labeled "$\|e\|_{L^2}$," "$\|e\|_{H^1}$," and "$\|e\|_{a_h}$," represent the errors in the $L^2$, $H^1$, and energy ($\|e\|_{a_h}$,) norms, respectively. The column labeled "EOC" denotes the experimental order of convergence. The last two columns provide the condition number of the system and the number of degrees of freedom (ndofs), respectively.

Figure 10 displays a plot illustrating the error convergence in the $L^2$, $H^1$, and energy norms for the CutCIP method (Laplace) with second-order accuracy.

Additionally, we compare the results with and without the ghost penalty in two different tests: a translation test and a convergence test. The translation test examines the evolution of the condition

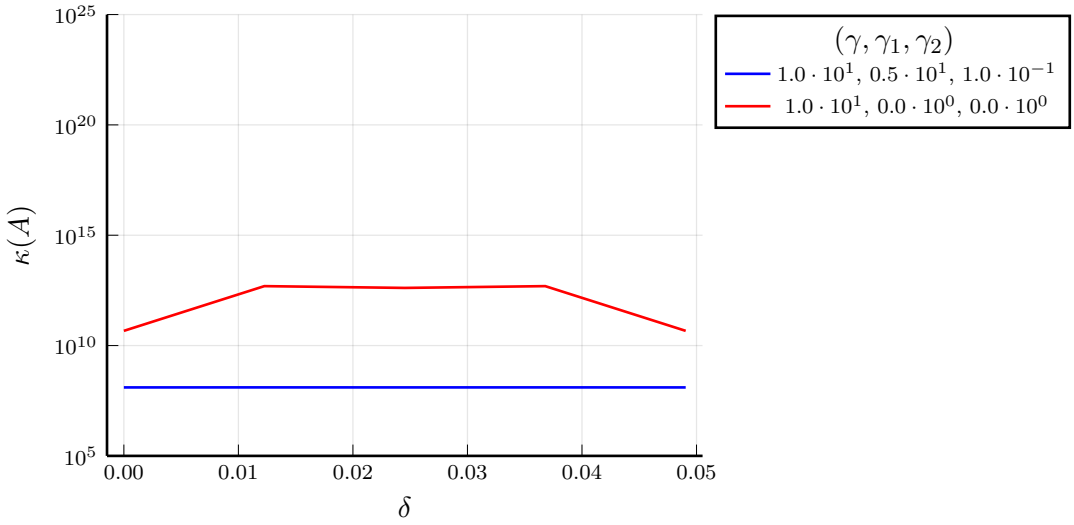


Figure 10: The plot presents the error in $L^2$, $H^1$ the energy norm ($\|e\|_{a_h,*}$) with order 2 of the CutCIP method (Laplace).

number and error number, as shown in Figure 11. The convergence test also investigates the condition number and error number, and its results are presented in Figure 11.

Overall, these numerical results provide insights into the performance and accuracy of the numerical method, showcasing the convergence behavior and the impact of the ghost penalty on the solution.

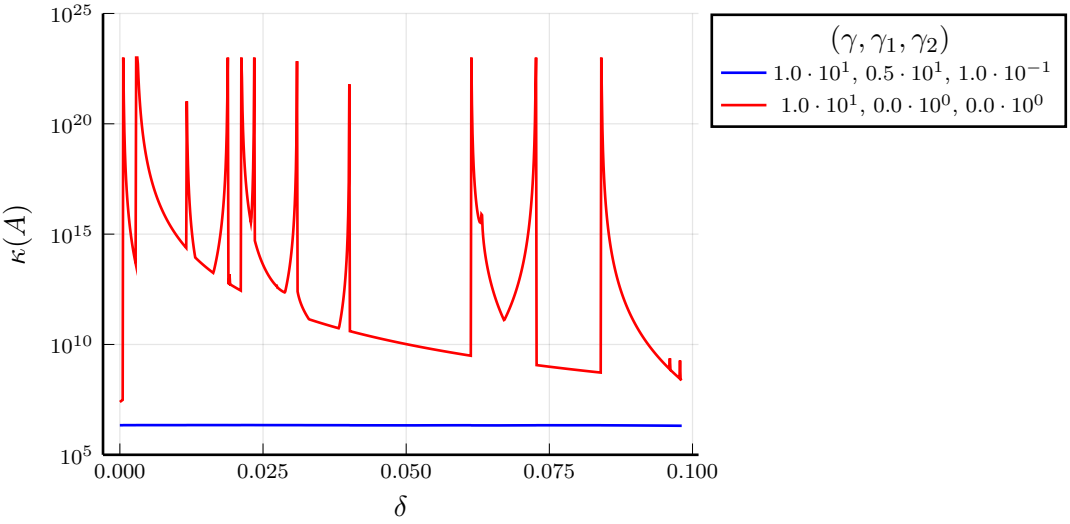


(a) Evolution of condition number

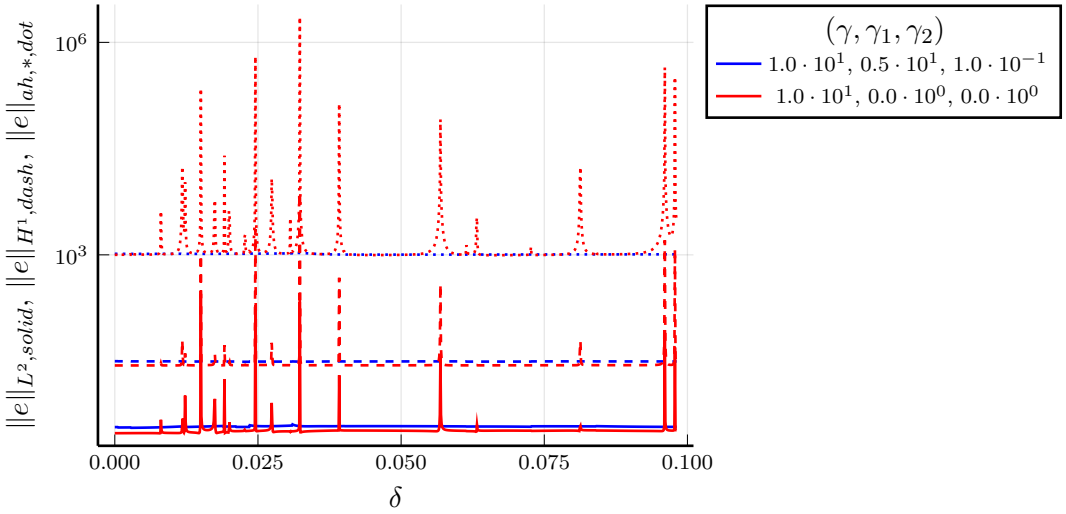


(b) Evolution of error number

Figure 11: Comparison of translation of circle with radius $R = 1$ from with 1000 steps for $n = 2^4$, $L = 1.11$ and $h = \frac{L}{n}$ s.t. $\delta \in [0, \sqrt{2}h]$. Here is the test specifically for without ghost penalty, $\gamma_1 = \gamma_2 = 0$ and with ghost penalty, $\gamma_1 = 5$ and $\gamma_2 = 0.1$.

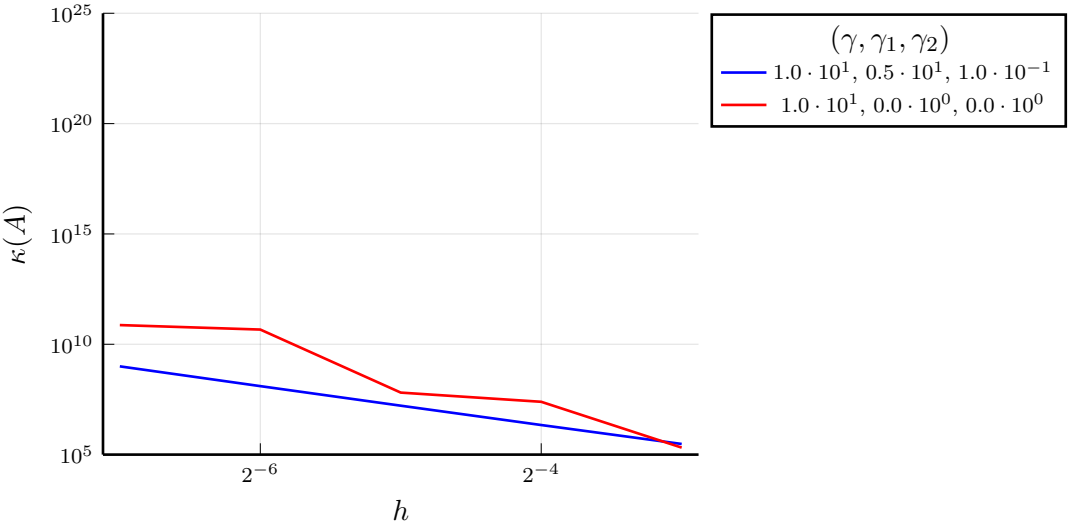


(a) Evolution of condition number

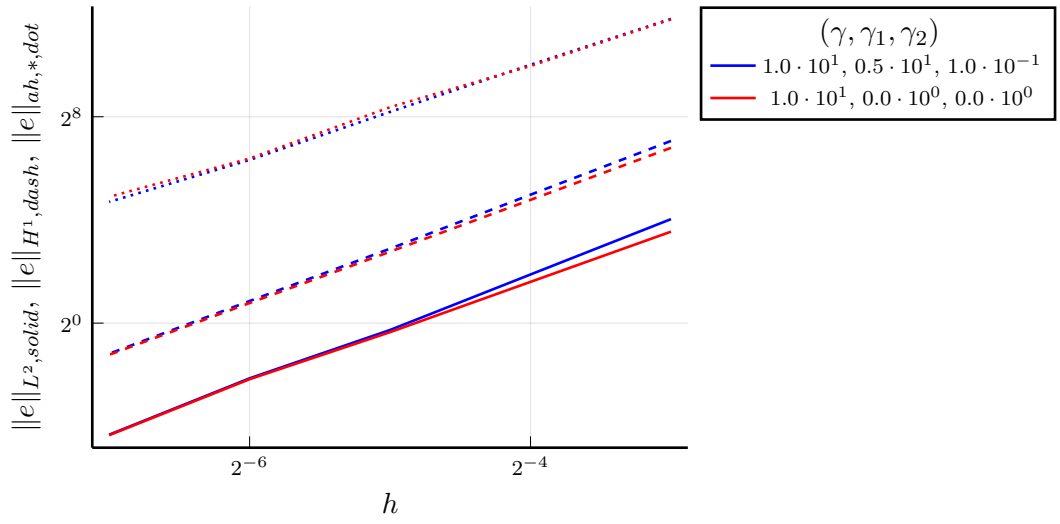


(b) Evolution of error number

Figure 12: Comparison of convergence test results with and without ghost penalty.

# References


[1] John W Cahn and John E Hilliard. "Free energy of a nonuniform system. I. Interfacial free energy". In: *The Journal of chemical physics* 28.2 (1958), pp. 258–267.

[2] John W Cahn and John E Hilliard. "Free energy of a nonuniform system. III. Nucleation in a two-component incompressible fluid". In: *The Journal of chemical physics* 31.3 (1959), pp. 688–699.

[3] John W Cahn. "On spinodal decomposition". In: *Acta metallurgica* 9.9 (1961), pp. 795–801.

[4] Jessica Bosch and Martin Stoll. "A fractional inpainting model based on the vector-valued Cahn–Hilliard equation". In: *SIAM Journal on Imaging Sciences* 8.4 (2015), pp. 2352–2382.

[5] David J Eyre. "Systems of cahn–hilliard equations". In: *SIAM Journal on Applied Mathematics* 53.6 (1993), pp. 1686–1712.

[6] Gyula I Tóth, Mojdeh Zarifi, and Bjørn Kvamme. "Phase-field theory of multicomponent incompressible Cahn-Hilliard liquids". In: *Physical Review E* 93.1 (2016), p. 013126.

[7] Alain Miranville. "The Cahn–Hilliard equation and some of its variants". In: *AIMS Mathematics* 2.3 (2017), pp. 479–544.

[8] Ingo Steinbach. "Phase-field models in materials science". In: *Modelling and simulation in materials science and engineering* 17.7 (2009), p. 073001.

[9] Long-Qing Chen. "Phase-field models for microstructure evolution". In: *Annual review of materials research* 32.1 (2002), pp. 113–140.

[10] Vittorio E Badalassi, Hector D Ceniceros, and Sanjoy Banerjee. "Computation of multiphase systems with phase field models". In: *Journal of computational physics* 190.2 (2003), pp. 371–397.

[11] Qing Li et al. "Lattice Boltzmann methods for multiphase flow and phase-change heat transfer". In: *Progress in Energy and Combustion Science* 52 (2016), pp. 62–105.

[12] Junseok Kim. "Phase-field models for multi-component fluid flows". In: *Communications in Computational Physics* 12.3 (2012), pp. 613–661.

[13] Jie Shen and Xiaofeng Yang. "A phase-field model and its numerical approximation for two-phase incompressible flows with different densities and viscosities". In: *SIAM Journal on Scientific Computing* 32.3 (2010), pp. 1159–1179.

[14] Seong Gyoon Kim, Won Tae Kim, and Toshio Suzuki. "Phase-field model for binary alloys". In: *Physical review e* 60.6 (1999), p. 7186.

[15] Blas Echebarria et al. "Quantitative phase-field model of alloy solidification". In: *Physical review E* 70.6 (2004), p. 061604.

[16] Charlotte Kuhn and Ralf Müller. "A continuum phase field model for fracture". In: *Engineering Fracture Mechanics* 77.18 (2010), pp. 3625–3634.

[17] Bin Li et al. "Phase-field modeling and simulation of fracture in brittle materials with strongly anisotropic surface energy". In: *International Journal for Numerical Methods in Engineering* 102.3-4 (2015), pp. 711–727.

[18] Andrea L Bertozzi, Selim Esedoglu, and Alan Gillette. "Inpainting of binary images using the Cahn–Hilliard equation". In: *IEEE Transactions on image processing* 16.1 (2006), pp. 285–291.

[19] Martin Burger, Lin He, and Carola-Bibiane Schönlieb. "Cahn–Hilliard inpainting and a generalization for grayvalue images". In: *SIAM Journal on Imaging Sciences* 2.4 (2009), pp. 1129–1167.

[20] Antun Lovro Brkić, Darko Mitrović, and Andrej Novak. "On the image inpainting problem from the viewpoint of a nonlocal Cahn-Hilliard type equation". In: *Journal of Advanced Research* 25 (2020), pp. 67–76.

[21] Scott Tremaine. "On the origin of irregular structure in Saturn's rings". In: *The Astronomical Journal* 125.2 (2003), p. 894.

[22] Abramo Agosti et al. "A Cahn-Hilliard–type equation with application to tumor growth dynamics". In: *Mathematical Methods in the Applied Sciences* 40.18 (2017), pp. 7598–7626.

[23] Vittorio Cristini et al. “Nonlinear simulations of solid tumor growth using a mixture model: invasion and branching”. In: *Journal of mathematical biology* 58 (2009), pp. 723–763.

[24] Ilya Levental, Kandice R Levental, and Frederick A Heberle. “Lipid rafts: controversies resolved, mysteries remain”. In: *Trends in cell biology* 30.5 (2020), pp. 341–353.

[25] John F Hancock. “Lipid rafts: contentious only from simplistic standpoints”. In: *Nature Reviews Molecular Cell Biology* 7.6 (2006), pp. 456–462.

[26] Sean Munro. “Lipid rafts: elusive or illusive?” In: *Cell* 115.4 (2003), pp. 377–388.

[27] Kai Simons and Elina Ikonen. “Functional rafts in cell membranes”. In: *nature* 387.6633 (1997), pp. 569–572.

[28] Ethan J Miller et al. “Divide and conquer: How phase separation contributes to lateral transport and organization of membrane proteins and lipids”. In: *Chemistry and Physics of Lipids* 233 (2020), p. 104985.

[29] Harald Garcke et al. “A coupled surface-Cahn–Hilliard bulk-diffusion system modeling lipid raft formation in cell membranes”. In: *Mathematical Models and Methods in Applied Sciences* 26.06 (2016), pp. 1149–1189.

[30] Vladimir Yushutin et al. “A computational study of lateral phase separation in biological membranes”. In: *International journal for numerical methods in biomedical engineering* 35.3 (2019), e3181.

[31] Dongsun Lee et al. “Physical, mathematical, and numerical derivations of the Cahn–Hilliard equation”. In: *Computational Materials Science* 81 (2014), pp. 216–225.

[32] Harald Garcke and Patrik Knopf. “Weak solutions of the Cahn–Hilliard system with dynamic boundary conditions: A gradient flow approach”. In: *SIAM Journal on Mathematical Analysis* 52.1 (2020), pp. 340–369.

[33] Helmut Abels and Mathias Wilke. “Convergence to equilibrium for the Cahn–Hilliard equation with a logarithmic free energy”. In: *Nonlinear Analysis: Theory, Methods & Applications* 67.11 (2007), pp. 3176–3193.

[34] Laurence Cherfils, Alain Miranville, and Sergey Zelik. “The Cahn-Hilliard equation with logarithmic potentials”. In: *Milan Journal of Mathematics* 79 (2011), pp. 561–596.

[35] Charles M Elliott and Zheng Songmu. “On the cahn-hilliard equation”. In: *Archive for Rational Mechanics and Analysis* 96 (1986), pp. 339–357.

[36] Daisuke Furihata. “A stable and conservative finite difference scheme for the Cahn-Hilliard equation”. In: *Numerische Mathematik* 87.4 (2001), pp. 675–699.

[37] Kelong Cheng et al. “An energy stable fourth order finite difference scheme for the Cahn–Hilliard equation”. In: *Journal of Computational and Applied Mathematics* 362 (2019), pp. 574–595.

[38] Chun Liu and Jie Shen. “A phase field model for the mixture of two incompressible fluids and its approximation by a Fourier-spectral method”. In: *Physica D: Nonlinear Phenomena* 179.3-4 (2003), pp. 211–228.

[39] Li-ping He and Yunxian Liu. “A class of stable spectral methods for the Cahn–Hilliard equation”. In: *Journal of Computational Physics* 228.14 (2009), pp. 5101–5110.

[40] Yibao Li et al. “A conservative numerical method for the Cahn–Hilliard equation with Dirichlet boundary conditions in complex domains”. In: *Computers & Mathematics with Applications* 65.1 (2013), pp. 102–115.

[41] Jie Shen and Xiaofeng Yang. “An efficient moving mesh spectral method for the phase-field model of two-phase flows”. In: *Journal of computational physics* 228.8 (2009), pp. 2978–2992.

[42] WM Feng et al. “A Fourier spectral moving mesh method for the Cahn–Hilliard equation with elasticity”. In: *Commun. Comput. Phys* 5.2-4 (2009), pp. 582–599.

[43] Charles M Elliott and Donald A French. “Numerical studies of the Cahn-Hilliard equation for phase separation”. In: *IMA Journal of Applied Mathematics* 38.2 (1987), pp. 97–128.

[44] Mario Kapl, Giancarlo Sangalli, and Thomas Takacs. “A family of C 1 quadrilateral finite elements”. In: *Advances in Computational Mathematics* 47 (2021), pp. 1–38.

[45] Peter Percell. “On cubic and quartic Clough–Tocher finite elements”. In: *SIaM Journal on numerical analysis* 13.1 (1976), pp. 100–103.

[46] John H Argyris, Isaac Fried, and Dieter W Scharpf. "The TUBA family of plate elements for the matrix displacement method". In: *The Aeronautical Journal* 72.692 (1968), pp. 701–709.

[47] Thomas JR Hughes, John A Cottrell, and Yuri Bazilevs. "Isogeometric analysis: CAD, finite elements, NURBS, exact geometry and mesh refinement". In: *Computer methods in applied mechanics and engineering* 194.39-41 (2005), pp. 4135–4195.

[48] Markus Kästner, Philipp Metsch, and Rene De Borst. "Isogeometric analysis of the Cahn–Hilliard equation–a convergence study". In: *Journal of Computational Physics* 305 (2016), pp. 360–371.

[49] Héctor Gómez et al. "Isogeometric analysis of the Cahn–Hilliard phase-field model". In: *Computer methods in applied mechanics and engineering* 197.49-50 (2008), pp. 4333–4352.

[50] Ying Zhao, Dominik Schillinger, and Bai-Xiang Xu. "Variational boundary conditions based on the Nitsche method for fitted and unfitted isogeometric discretizations of the mechanically coupled Cahn–Hilliard equation". In: *Journal of Computational Physics* 340 (2017), pp. 177–199.

[51] Christopher Zimmermann et al. "An isogeometric finite element formulation for phase transitions on deforming surfaces". In: *Computer Methods in Applied Mechanics and Engineering* 351 (2019), pp. 441–477.

[52] Paola F Antonietti et al. "A Cˆ1 virtual element method for the Cahn–Hilliard equation with polygonal meshes". In: *SIAM Journal on Numerical Analysis* 54.1 (2016), pp. 34–56.

[53] Susanne Brenner. *C0 Interior Penalty Methods*. Springer International Publishing, 2012. URL: https://link.springer.com/content/pdf/10.1007/978-3-642-23914-4_2.pdf.

[54] Susanne C Brenner et al. "A Quadratic Cˆ0 Interior Penalty Method for Linear Fourth Order Boundary Value Problems with Boundary Conditions of the Cahn–Hilliard Type". In: *SIAM Journal on Numerical Analysis* 50.4 (2012), pp. 2088–2110.

[55] Susanne C Brenner et al. "A quadratic Cˆ0 interior penalty method for the displacement obstacle problem of clamped Kirchhoff plates". In: *SIAM Journal on Numerical Analysis* 50.6 (2012), pp. 3329–3350.

[56] Lin Mu, Junping Wang, and Xiu Ye. "Weak Galerkin finite element methods for the biharmonic equation on polytopal meshes". In: *Numerical Methods for Partial Differential Equations* 30.3 (2014), pp. 1003–1029.

[57] Emmanuil H Georgoulis and Paul Houston. "Discontinuous Galerkin methods for the biharmonic problem". In: *IMA journal of numerical analysis* 29.3 (2009), pp. 573–594.

[58] Daniele Antonio Di Pietro and Alexandre Ern. *Mathematical aspects of discontinuous Galerkin methods*. Vol. 69. Springer Science & Business Media, 2011.

[59] Garth N Wells, Ellen Kuhl, and Krishna Garikipati. "A discontinuous Galerkin method for the Cahn–Hilliard equation". In: *Journal of Computational Physics* 218.2 (2006), pp. 860–877.

[60] Xiaobing Feng and Ohannes Karakashian. "Fully discrete dynamic mesh discontinuous Galerkin methods for the Cahn-Hilliard equation of phase transition". In: *Mathematics of computation* 76.259 (2007), pp. 1093–1117.

[61] Richard S Falk. "Approximation of the biharmonic equation by a mixed finite element method". In: *SIAM Journal on Numerical Analysis* 15.3 (1978), pp. 556–567.

[62] Philippe G Ciarlet and Pierre-Arnaud Raviart. "A mixed finite element method for the biharmonic equation". In: *Mathematical aspects of finite elements in partial differential equations* (1974), pp. 125–145.

[63] Thirupathi Gudi, Neela Nataraj, and Amiya K Pani. "Mixed discontinuous Galerkin finite element method for the biharmonic equation". In: *Journal of Scientific Computing* 37 (2008), pp. 139–161.

[64] Xiao-liang Cheng, Weimin Han, and Hong-ci Huang. "Some mixed finite element methods for biharmonic equation". In: *Journal of computational and applied mathematics* 126.1-2 (2000), pp. 91–109.

[65] Volker John et al. *Finite element methods for incompressible flow problems*. Vol. 51. Springer, 2016.

[66] Xiaobing Feng and Andreas Prohl. "Error analysis of a mixed finite element method for the Cahn-Hilliard equation". In: *Numerische Mathematik* 99 (2004), pp. 47–84.

[67] Amanda E Diegel, Xiaobing H Feng, and Steven M Wise. "Analysis of a mixed finite element method for a Cahn–Hilliard–Darcy–Stokes system". In: *SIAM Journal on Numerical Analysis* 53.1 (2015), pp. 127–152.

[68] Susanne C Brenner, Amanda E Diegel, and Li-Yeng Sung. "A robust solver for a mixed finite element method for the Cahn–Hilliard equation". In: *Journal of Scientific Computing* 77 (2018), pp. 1234–1249.

[69] Florent Chave et al. "A Hybrid High-Order Method for the Cahn–Hilliard problem in Mixed Form". In: *SIAM Journal on Numerical Analysis* 54.3 (2016), pp. 1873–1898.

[70] Emmanuel Y Medina et al. "A stabilized hybrid discontinuous Galerkin method for the Cahn–Hilliard equation". In: *Journal of Computational and Applied Mathematics* 406 (2022), p. 114025.

[71] Erik Burman et al. "CutFEM: discretizing geometry and partial differential equations". In: *International Journal for Numerical Methods in Engineering* 104.7 (2015), pp. 472–501.

[72] Ying Cai, Jinru Chen, and Nan Wang. "A Nitsche mixed extended finite element method for the biharmonic interface problem". In: *Mathematics and Computers in Simulation* 203 (2023), pp. 112–130.

[73] Yan Chen, Ruo Li, and Qicheng Liu. "An arbitrary order Reconstructed Discontinuous Approximation to Biharmonic Interface Problem". In: *arXiv preprint arXiv:2305.03430* (2023).

[74] Efthymios N Karatzas and Gianluigi Rozza. "A reduced order model for a stable embedded boundary parametrized Cahn–Hilliard phase-field system based on cut finite elements". In: *Journal of Scientific Computing* 89.1 (2021), p. 9.

[75] Santiago Badia, Francesc Verdugo, and Alberto F Martín. "The aggregated unfitted finite element method for elliptic problems". In: *Computer Methods in Applied Mechanics and Engineering* 336 (2018), pp. 533–553.

[76] Santiago Badia, Eric Neiva, and Francesc Verdugo. "Linking ghost penalty and aggregated unfitted methods". In: *Computer Methods in Applied Mechanics and Engineering* 388 (2022), p. 114232.

[77] Alexandre Ern Daniele Antonio Di Pietro. "Mathematical Aspects of Discontinuous Galerkin Methods". In: (2012). URL: https://link.springer.com/content/pdf/10.1007/978-3-642-23914-4_2.pdf.

[78] Anita Hansbo, Peter Hansbo, and Mats G Larson. "A finite element method on composite grids based on Nitsche's method". In: *ESAIM: Mathematical Modelling and Numerical Analysis* 37.3 (2003), pp. 495–514.

[79] A. Ern and J.L. Guermond. *Theory and Practice of Finite Elements*. Applied Mathematical Sciences. Springer New York, 2004, pp. 69–70. ISBN: 9780387205748. URL: https://books.google.no/books?id=CCjm79FbJbcC.

[80] Ceren Gürkan and André Massing. "A stabilized cut discontinuous Galerkin framework for elliptic boundary value and interface problems". In: *Computer Methods in Applied Mechanics and Engineering* 348 (2019), pp. 466–499.

[81] Francesc Verdugo and Santiago Badia. "The software design of Gridap: A Finite Element package based on the Julia JIT compiler". In: *Computer Physics Communications* 276 (July 2022), p. 108341. DOI: 10.1016/j.cpc.2022.108341. URL: https://doi.org/10.1016/j.cpc.2022.108341.

[82] Jeff Bezanson et al. "Julia: A fresh approach to numerical computing". In: *SIAM Review* 59.1 (2017), pp. 65–98. DOI: 10.1137/141000671. URL: https://epubs.siam.org/doi/10.1137/141000671.